

Annual Review of Condensed Matter Physics Odd Viscosity and Odd Elasticity

Michel Fruchart,¹ Colin Scheibner,¹ and Vincenzo Vitelli^{1,2}

- ¹James Franck Institute and Department of Physics, The University of Chicago, Chicago, Illinois, USA
- ²Kadanoff Center for Theoretical Physics, The University of Chicago, Chicago, Illinois, USA; email: vitelli@uchicago.edu



www.annualreviews.org

- Download figures
- · Navigate cited references
- Keyword search
- · Explore related articles
- Share via email or social media

Annu. Rev. Condens. Matter Phys. 2023. 14:471-510

The Annual Review of Condensed Matter Physics is online at commatphys.annualreviews.org

https://doi.org/10.1146/annurev-conmatphys-040821-125506

Copyright © 2023 by the author(s). This work is licensed under a Creative Commons Attribution 4.0 International License, which permits unrestricted use, distribution, and reproduction in any medium, provided the original author and source are credited. See credit lines of images or other third-party material in this article for license information.



Keywords

continuum mechanics, fluid mechanics, nonequilibrium, active matter, hydrodynamics, rheology

Abstract

Elasticity typically refers to a material's ability to store energy, whereas viscosity refers to a material's tendency to dissipate it. In this review, we discuss fluids and solids for which this is not the case. These materials display additional linear response coefficients known as odd viscosity and odd elasticity. We first introduce odd viscosity and odd elasticity from a continuum perspective, with an emphasis on their rich phenomenology, including transverse responses, modified dislocation dynamics, and topological waves. We then provide an overview of systems that display odd viscosity and odd elasticity. These systems range from quantum fluids and astrophysical gases to active and driven matter. Finally, we comment on microscopic mechanisms by which odd viscosity and odd elasticity arise.

1. INTRODUCTION

Continuum theories are phenomenological tools that allow us to understand and manipulate the world around us (1–3). Classical field theories such as elasticity and fluid mechanics have been built upon certain symmetries and conservation laws that are suitable for everyday materials such as water in rivers or steel beams in bridges. Examples include time-reversal invariance, mirror reflection symmetry, or conservation of energy and angular momentum. Yet not all systems are subject to these constraints: Counterexamples range from biological tissues and astrophysical gases to quantum fluids. In this review, we analyze minimal extensions of fluid and solid mechanics that arise when the microscopic constituents of a medium do not follow these usual symmetries and conservation laws. As a consequence, the continuum theories acquire new terms that take into account the collective effect of the broken symmetries. The advantage of this perspective is that we obtain universal effective theories that describe an array of systems that span many areas of research. The drawback is that these universal theories, by nature, do not describe every detail of each system.

The key feature shared by all the systems in this review is that their evolution is governed by forces between adjacent parcels of a continuous medium. This physics is captured mathematically by the stress tensor,

$$\sigma_{ii} = C_{iik\ell} \partial_{\ell} u_k + \eta_{iik\ell} \partial_{\ell} \dot{u}_k + \cdots,$$
 1.

which summarizes the surface forces between material elements. (Throughout this review, repeated indices are summed over unless otherwise mentioned.) In terms of the stresses, the internal forces in the medium are given by $f_i = \partial_j \sigma_{ij}$. The elasticity tensor $C_{ijk\ell}$ is the proportionality coefficient between the stress tensor and the displacement gradient $e_{k\ell} = \partial_\ell u_k$. The viscosity tensor $\eta_{ijk\ell}$ is the proportionality coefficient between the stress and the velocity gradient $\dot{e}_{k\ell} = \partial_\ell \dot{u}_k$. Equation 1 gives a mechanical definition of elasticity and viscosity. In usual fluids and solids, respectively, these coefficients can be expressed as

$$C_{ijk\ell} = \frac{\delta^2 F}{\delta(\partial_j u_i)\delta(\partial_\ell u_k)} \quad \text{and} \quad \eta_{ijk\ell} = \frac{T\delta^2 \dot{S}}{\delta(\partial_j \dot{u}_i)\delta(\partial_\ell \dot{u}_k)} \quad \text{(usually)},$$

where F is the free energy of the elastic medium, \hat{S} the rate of entropy production of the fluid, and T is the temperature. Equation 2 summarizes the usual meaning of elasticity and viscosity: Elasticity usually describes the reversible storage of energy, whereas viscosity describes its irreversible dissipation. When Equation 2 holds, the elasticity and viscosity tensors obey the symmetries

$$C_{ijk\ell} = C_{k\ell ij}$$
 and $\eta_{ijk\ell} = \eta_{k\ell ij}$ (usually).

This review discusses situations in which Equation 3 is not valid, i.e., situations in which the elasticity and viscosity tensors are not symmetric:

$$C_{ijk\ell} \neq C_{k\ell ij}$$
 and $\eta_{ijk\ell} \neq \eta_{k\ell ij}$ (more generally).

The antisymmetric parts of $C_{ijk\ell}$ and $\eta_{ijk\ell}$ in Equation 4 are henceforth referred to as "odd" because they flip sign upon exchanging the pair of indices ij with $k\ell$. As we explain in Sections 2.3 and 3.3, odd elasticity is generally associated with microscopic nonconservative forces, whereas odd viscosity is usually associated with microscopic dynamics that do not obey time-reversal symmetry $(t \to -t)$. Both happen to be often related to the breaking of mirror symmetry (also called parity), in which a single coordinate is flipped (e.g., $x \to -x$). These coefficients arise in systems spanning scales, from quantum fluids to geophysical flows, and tabletop experiments with driven and active particles.

2. ODD VISCOSITY

2.1. What Is Viscosity?

When you stir a fluid, such as water or honey, the fluid resists the motion you are trying to impart. This is due to viscosity, which captures the resistance of the fluid against inhomogeneities in its velocity field. Honey is more viscous than water, so stirring honey requires more work than stirring water. When velocity gradients are present, forces appear between neighboring fluid parcels that tend to make their velocities equal. Formally, this is described by the Navier–Stokes equation,

$$\rho D_t v_i = \partial_i \sigma_{ii} + f_i, \qquad 5.$$

in which $D_t = \partial_t + v_k \partial_k$ is the convective derivative, ρ is the density, $\mathbf{v}(t, \mathbf{x})$ is the velocity field, f_i are external body forces, and

$$\sigma_{ij} = \sigma_{ij}^{h} + \eta_{ijk\ell} \, \partial_{\ell} v_{k} \tag{6}$$

is the stress tensor, which describes the forces between fluid parcels. We have decomposed the stress tensor into so-called hydrostatic stresses $\sigma^{\rm h}_{ij}$ that are present even when the fluid is at rest (in usual fluids, $\sigma^{\rm h}_{ij} = -p\delta_{ij}$, where p is the pressure), and viscous stresses $\sigma^{\rm vis}_{ij} = \eta_{ijk\ell}\partial_\ell v_k$, which are induced by velocity gradients. The coefficient of proportionality $\eta_{ijk\ell}$ between velocity gradients and the stress is called the viscosity tensor. The divergence of the viscous stress tensor is a force density, $f_i^{\rm vis} = \partial_j \eta_{ijk\ell} \partial_\ell v_k$, that enters the Navier–Stokes equation. In an isotropic, incompressible fluid at equilibrium, it takes the familiar form $f_i^{\rm vis} = \eta \ \Delta v_i$, where η is the shear viscosity.

As one may expect from the examples of water and honey, viscosity measures how much mechanical energy is converted into heat by the friction between layers of fluid. The rate of loss of mechanical energy by viscous dissipation per unit volume is (2, 4)

$$\dot{w} = \sigma_{ij}^{\text{vis}} \partial_j v_i = \eta_{ijk\ell}(\partial_j v_i)(\partial_\ell v_k) = \eta_{ijk\ell}^{\text{S}}(\partial_j v_i)(\partial_\ell v_k).$$
 7.

From this expression, we see that only the symmetric part $\eta_{ijk\ell}^S = [\eta_{ijk\ell} + \eta_{k\ell ij}]/2$ of the viscosity tensor contributes to dissipation. The antisymmetric part,

$$\eta_{ijk\ell}^{A} = [\eta_{ijk\ell} - \eta_{k\ell ij}]/2$$
 (odd viscosity tensor), 8.

drops out. Therefore, the antisymmetric part of the viscosity tensor $\eta^{A}_{ijk\ell}$ describes nondissipative viscosities, which are called odd viscosities (5). Depending on the context, odd viscosity is known by other names, such as Hall viscosity, gyroviscosity, Lorentz shear modulus, and the Senftleben–Beenakker effect.

2.1.1. Two-dimensional fluids with odd viscosity. In two dimensions, the viscosity tensor $\eta_{ijk\ell}$ contains $2^4 = 16$ independent components. To keep track of them, it is useful to introduce a physically intuitive basis for stress and strain rate, summarized in **Table 1** and in the **Supplemental Text**. In this notation, the velocity gradient $\dot{e}_{k\ell} = \partial_{\ell} v_k$ and stress σ_{ij} are represented by vectors \dot{e}_{α} and σ_{α} , respectively, and the viscosity tensor $\eta_{ijk\ell}$ is represented by a four-by-four matrix $\eta_{\alpha\beta}$ (α , $\beta = 0, \ldots, 3$). In an isotropic fluid (i.e., one with no distinguished axis), the stress-velocity

Odd viscosity: nondissipative component of the viscosity tensor, contained in its antisymmetric part

Hall viscosity:

synonym of odd viscosity in the context of condensed matter physics

Supplemental Material >

¹In this review, we focus on Newtonian fluids, in which the viscous stresses are assumed to be linearly proportional to the velocity gradients, and we treat the viscosities as constants. In general, the viscous stress tensor can be a nonlinear function of the velocity gradients. Within linear response, the stress tensor can also depend on gradients of other fields (temperature, density, etc.). In general, the stress tensor can be a nonlinear function of all the fields.

Deformation	Deformation rate	Stress	Geometric meaning
$e_0 = \square = \partial_x u_x + \partial_y u_y$	$\dot{e}_0 = \dot{\underline{\mathbf{n}}} = \partial_x v_x + \partial_y v_y$	$\sigma_0 = \bigoplus = [\sigma_{xx} + \sigma_{yy}]/2$	isotropic area change
$e_1 = \bigcirc = \partial_x u_y - \partial_y u_x$	$\dot{e}_1 = \dot{\Diamond} = \partial_x v_y - \partial_y v_x$	$\sigma_1 = \bigcirc = [\sigma_{yx} - \sigma_{xy}]/2$	rotation
$e_2 = \square = \partial_x u_x - \partial_y u_y$	$\dot{e}_2 = \dot{} = \partial_x v_x - \partial_y v_y$	$\sigma_2 = \bigoplus = [\sigma_{xx} - \sigma_{yy}]/2$	pure shear 1
$e_3 = \square = \partial_x u_y + \partial_y u_x$	$\dot{e}_3 = \dot{\underline{b}} = \partial_x v_y + \partial_y v_x$	$\sigma_3 = \mathbf{s} = [\sigma_{xy} + \sigma_{yx}]/2$	pure shear 2

A pure shear (rate) corresponds to a (rate of) change in shape without a change in volume or orientation. Shear 1 describes a horizontal elongation and vertical compression, whereas shear 2 describes elongation along the 45° direction and compression along the -45° direction. We note that $\dot{e}_0 = \nabla \cdot \boldsymbol{v}$ and $\dot{e}_1 = \boldsymbol{\omega}$ is vorticity. The stresses are the conjugate forces to these deformations and have similar interpretations. In particular, σ_0 includes pressure. The antisymmetric stress σ_1 is discussed in the sidebar titled Antisymmetric Stress.

'≸upplemental Material >

gradient relation takes the following form (6; see also the Supplemental Text):

Here, p is the hydrostatic pressure, and τ is a hydrostatic torque that can arise, for instance, when particles have transverse (i.e., noncentral) forces (see the sidebar titled Antisymmetric Stress). The matrix $\eta_{\alpha\beta}$ has six independent coefficients. The shear, bulk, and rotational viscosities, η , ζ , and η^R , respectively, arise in usual fluids.² The coefficients η^A and η^B couple compression and rotation, whereas the odd shear viscosity η^o couples the two independent shears. In standard tensor notation, the viscosity tensor in Equation 9 reads as

$$\eta_{ijk\ell} = \zeta \, \delta_{ij} \delta_{k\ell} - \eta^{A} \epsilon_{ij} \delta_{k\ell} - \eta^{B} \delta_{ij} \epsilon_{k\ell} + \eta^{R} \epsilon_{ij} \epsilon_{k\ell}
+ \eta (\delta_{ik} \delta_{i\ell} + \delta_{i\ell} \delta_{ik} - \delta_{ij} \delta_{k\ell}) + \eta^{\circ} (\epsilon_{ik} \delta_{i\ell} + \epsilon_{i\ell} \delta_{ik}),$$
10.

ANTISYMMETRIC STRESS

The stress tensor of fluids and solids composed of particles with noncentral interactions can exhibit an antisymmetric part, the antisymmetric stress $\sigma_{ij}^A = \frac{1}{2}[\sigma_{ij} - \sigma_{ji}]$ (6–8). This effect is distinct from odd viscosity and odd elasticity but often coexists with them. Mechanically, the antisymmetric stress corresponds to a torque density $\tau_i = \frac{1}{2}\epsilon_{ijk}\sigma_{jk}^A$, and it can arise, for instance, in fluids and solids made of spinning particles. Odd viscosity and elasticity can contribute to the antisymmetric stress, e.g., through η^A in Equation 9 and A in Equation 28. However, an antisymmetric stress can exist even in the absence of velocity or displacement gradient, in which case it is part of the so-called hydrostatic stress in fluids and of the so-called prestress in solids. In addition, antisymmetric stresses can also be generated by other mechanisms (distinct from odd elasticity or viscosity), such as passive Cosserat elasticity (9) or rotational viscosities (such as η^R in Equation 9; see also Reference 10). Note that the phrase "odd stress" (or "Hall stress") has been variously used in the literature to refer to either antisymmetric stress or any stress due to odd elasticity or viscosity.

²The shear viscosity η is the most familiar. The bulk viscosity ζ does not appear in the equations of motion of incompressible flows (because $\partial_i v_i = 0$). The rotational viscosity is also often neglected because it typically disappears from the equation of motion on a short timescale corresponding to the equilibration of internal angular momentum (11, their chapter XII, section 1).

where δ_{ij} and ϵ_{ij} denote the Kronecker delta and the Levi–Civita symbol (with $\epsilon_{xy} = 1$). The full Navier–Stokes equation then reads as³

$$\rho D_t \boldsymbol{v} = \nabla \cdot \boldsymbol{\sigma}^{h} + (\zeta - \eta^{R}) \nabla (\nabla \cdot \boldsymbol{v}) + (\eta + \eta^{R}) \Delta \boldsymbol{v} + (\eta^{o} + \eta^{B}) \boldsymbol{\epsilon} \cdot \Delta \boldsymbol{v} - (\eta^{A} + \eta^{B}) \boldsymbol{\epsilon} \cdot \nabla (\nabla \cdot \boldsymbol{v}),$$

in which $\nabla \times \mathbf{v} = \epsilon_{ij} \partial_i v_j$. The symmetry $\eta_{ijk\ell} = \eta_{k\ell ij}$ is equivalent to the symmetry $\eta_{\alpha\beta} = \eta_{\beta\alpha}$ of the matrix in Equation 9. Hence, having no odd viscosities ($\eta^A_{ijk\ell} = 0$) amounts to having $\eta^A = \eta^B$ and $\eta^o = 0$. By coincidence, it also turns out that η^A , η^B , and η^o all violate mirror symmetry. Hence, in order to have odd viscosities in 2D isotropic fluids, it is necessary that some physical ingredient breaks mirror symmetry, such as an external magnetic field or particles that all rotate in the same direction.

Anisotropic 2D fluids can have more odd viscosities (14, 18): This has been discussed in the context of nematic systems (18–20) as well as in solid-state physics, where the viscosity tensor can be constrained by the crystallographic symmetries of the underlying lattice (13, 14, 21–23). In the language of rheology, odd viscosity can be expressed in terms of the so-called normal stress difference (more precisely, the part that is odd in shear rate; see Reference 24 for details). Finally, we note that odd viscosities have also been studied in relativistic fluids (25, 26) and on curved surfaces (27, 28).

2.1.2. Three-dimensional fluids with odd viscosity. In three dimensions, the situation is more complex. The tensor $\eta_{ijk\ell}$ has $3^4 = 81$ independent components. It turns out that there are no odd viscosities compatible with spatial isotropy, implying that an odd viscous fluid in three dimensions must have (at the minimum) a preferred axis (4). A simple way to obtain such a preferred axis is to apply a magnetic field to the system, or to rotate it (this can indeed produce odd viscosity; see Section 2.5.1). In this case, the system still has cylindrical symmetry, and there are 8 independent nondissipative (i.e., odd) viscosities, 6 of which require parity to be broken (there are also 11 dissipative viscosities, 3 of which require parity to be broken; see the **Supplemental Text**); a full classification is given in Reference 4. This highlights that nondissipative viscosities and parity-violating viscosities are distinct notions. Even if we restrict our attention to shear viscosities in systems with cylindrical symmetry, two independent odd shear viscosities can exist, and have been measured experimentally (see Section 2.4.1). Like in two dimensions, point group symmetries of the underlying crystal further constrain the viscosity tensor in solid-state systems (14, 21, 29).

2.2. How Does Odd Viscosity Affect Flows?

As depicted in **Figure 1**, odd viscosity can have pronounced effects on fluid flows. Below, we detail how odd viscosity can enter the Navier-Stokes equations and modify their solutions.

Supplemental Material >

³From the point of view of the bulk Navier-Stokes equations, the six viscosities compatible with rotation invariance are redundant: There are only four independent coefficients. The equations are invariant when the viscosities are transformed as $\eta^A \to \eta^A + \alpha$, $\eta^B \to \eta^B - \alpha$, $\eta^o \to \eta^o + \alpha\zeta \to \zeta + \beta$, $\eta \to \eta - \beta$, $\eta^R \to \eta^R + \beta$, for arbitrary α and β . This ambiguity can be resolved if the stress tensor can be directly measured or imposed (e.g., through boundary conditions). See References 8, 12–16, and 17 for more details. Note also that different forms of the Navier-Stokes equation can be obtained using the vector calculus identity $\epsilon \cdot \nabla(\nabla \times v) = \nabla(\nabla \cdot v) - \Delta v$ for 2D vector fields.

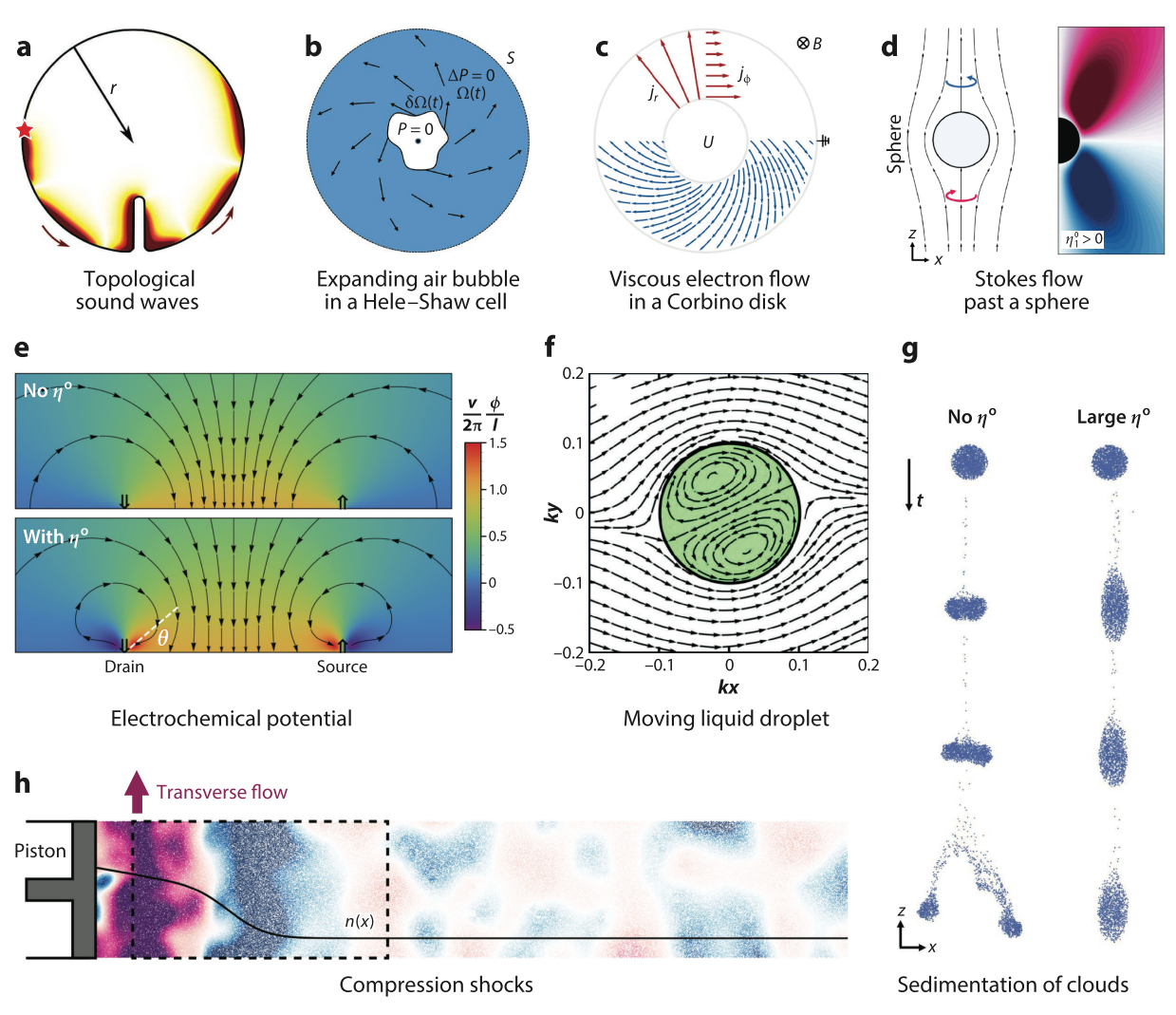


Figure 1

Phenomenological consequences of odd viscosity. (a) Topological sound waves arise from a combination of the Coriolis/Lorentz force and odd viscosity. Panel adapted with permission from Reference 40; copyright 2019 American Physical Society. (b) A chiral flow arises when a bubble expands inside a Hele–Shaw cell filled with a 3D odd viscous fluid. The flow acquires a circulation far from the bubble (represented by *spiraling arrows*) as a result of odd viscosities. Panel adapted from Reference 41. (c) A chiral flow arises in a Corbino disk filled with an odd viscous electron fluid under magnetic field. The electric current (in *blue*) between the inner and the outer disks spirals, because it has both a longitudinal and a transverse component (in *red*) with a ratio $j_{\phi}/j_r = \eta^{\circ}/\eta$. Panel adapted with permission from Reference 42; copyright 2019 American Physical Society. (d) The Stokes flow past a sphere develops an azimuthal component (*blue* and *pink arrows*) in an odd viscous fluid. On the right, the color represents the azimuthal component of the velocity (*red* and *blue* are opposite signs). Panel adapted from Reference 4. (e) Odd viscosity modifies the electrochemical potential near sources and drains in inhomogeneous charge flows in solid-state systems. Panel adapted with permission from Reference 43; copyright 2017 American Physical Society. (f) A moving liquid droplet consisting of an odd viscous fluid (*green*) in a normal liquid exhibits a nonaxisymmetric flow. Panel adapted from Reference 44. (g) An instability in the sedimentation of clouds of particles is suppressed by odd viscosity. Panel adapted from Reference 4. (b) A transverse flow appears in a compression shock in an odd viscous fluid. The color represents the transverse component of the velocity (vertical in the picture; *red* and *blue* are opposite signs). Panel adapted with permission from Reference 6; copyright 2021 Springer Nature.

2.2.1. Incompressible two-dimensional flows. Let us first consider the case of an incompressible (low Mach number⁴) 2D flow and consider only shear viscosities η and η °. The Navier–Stokes equations for such a system are

$$\rho D_t \mathbf{v} = -\nabla p + \eta \Delta \mathbf{v} + \eta^{\circ} \boldsymbol{\epsilon} \cdot \Delta \mathbf{v}, \qquad 11.$$

with $\nabla \cdot \mathbf{v} = 0$. In Equation 11, odd viscosity induces a viscous force perpendicular to the force one would generally expect from shear viscosity (the matrix $\boldsymbol{\epsilon}$ performs a clockwise rotation by 90°). Because of the incompressibility of the fluid, the odd viscous term $\eta^{\circ} \boldsymbol{\epsilon} \cdot \Delta \mathbf{v}$ can be incorporated in an effective pressure (30, 31),

$$p' = p - \eta^{\circ} \omega, \tag{12}$$

where $\omega = \epsilon_{k\ell} \partial_k v_\ell$ is the vorticity of the fluid, and we used the identity $\epsilon \Delta v = \nabla \omega$ for incompressible flows. We can therefore map the Navier–Stokes equation with odd viscosity (Equation 11) onto an effective system $\rho D_t v' = -\nabla p' + \eta \Delta v'$ without odd viscosity, with v' = v. This fact has an important consequence: When boundary conditions only involve the velocity of the fluid, the velocity field in a 2D fluid with and without η° are indistinguishable.

As an illustration, let us consider a 2D Poiseuille flow in which a fluid flows through a channel under a constant pressure gradient. In a normal fluid ($\eta^{o} = 0$), the velocity field is (32)

$$\mathbf{v} = \frac{G}{2\eta} y(b - y)\hat{\mathbf{e}}_x, \tag{13}$$

where G is the pressure gradient in the direction x (with unit vector \hat{e}_x), b is the height of the channel, and η is the (normal) shear viscosity. It satisfies the no-slip boundary conditions $\mathbf{v} = 0$ (which do not involve the stress) at the walls. The vorticity is given by $\omega = \partial_x v_y - \partial_y v_x = -G/[2\eta](b-2y)$. We now consider a fluid with odd viscosity in the same geometry. Recall that the velocity field is not modified by the presence of odd viscosity (nor is the vorticity). The pressure, however, is modified. Using Equation 12, we obtain

$$p = p' + \eta^{\circ} \omega = p' - \frac{G\eta^{\circ}}{2n}(b - 2y),$$
 14.

in which p' is the pressure in the system without odd viscosity. The transverse pressure difference, measured between the bottom and the top of the channel, is then⁶

$$\Delta p = p(b) - p(0) = G h \frac{\eta^{\circ}}{\eta}$$
 15.

as the pressure p'(y) of the Poiseuille flow without odd viscosity is up–down symmetric. A slightly more elaborate version of this method has been used to measure odd viscosities in 3D polyatomic gases (33–38; see **Figure 2***a* and Section 2.4.1).

2.2.2. Compressible flows. The effect of η° can be more dramatic in compressible flows. When odd viscosity is present in weakly compressible flows (at low Mach number), one expects vorticity

⁴The Mach number Ma = U/c is the ratio of a characteristic velocity of the fluid U by the speed of sound in the fluid c. Usually, a fluid can be considered incompressible when $Ma \ll 1$. In odd fluids, the additional condition $Ma^2/Re^o \ll 1$ can in certain conditions be required (30), where Re^o is the odd Reynolds number defined in Footnote 8.

⁵ In dilute systems, the rotational viscosities η^{A} and η^{B} are small and may be neglected (6).

⁶In the 2D incompressible system, the difference between normal forces at the top and bottom wall, $\sigma_{yy}(b) - \sigma_{yy}(0)$, does not capture odd viscosity, because in this geometry $\sigma_{yy}(y) = -p - \eta^{\circ} \partial_y v_x = -p'(y)$ is unchanged compared to the case with $\eta^{\circ} = 0$. The changes from pressure and viscous shear stress that contribute to these normal forces compensate exactly.

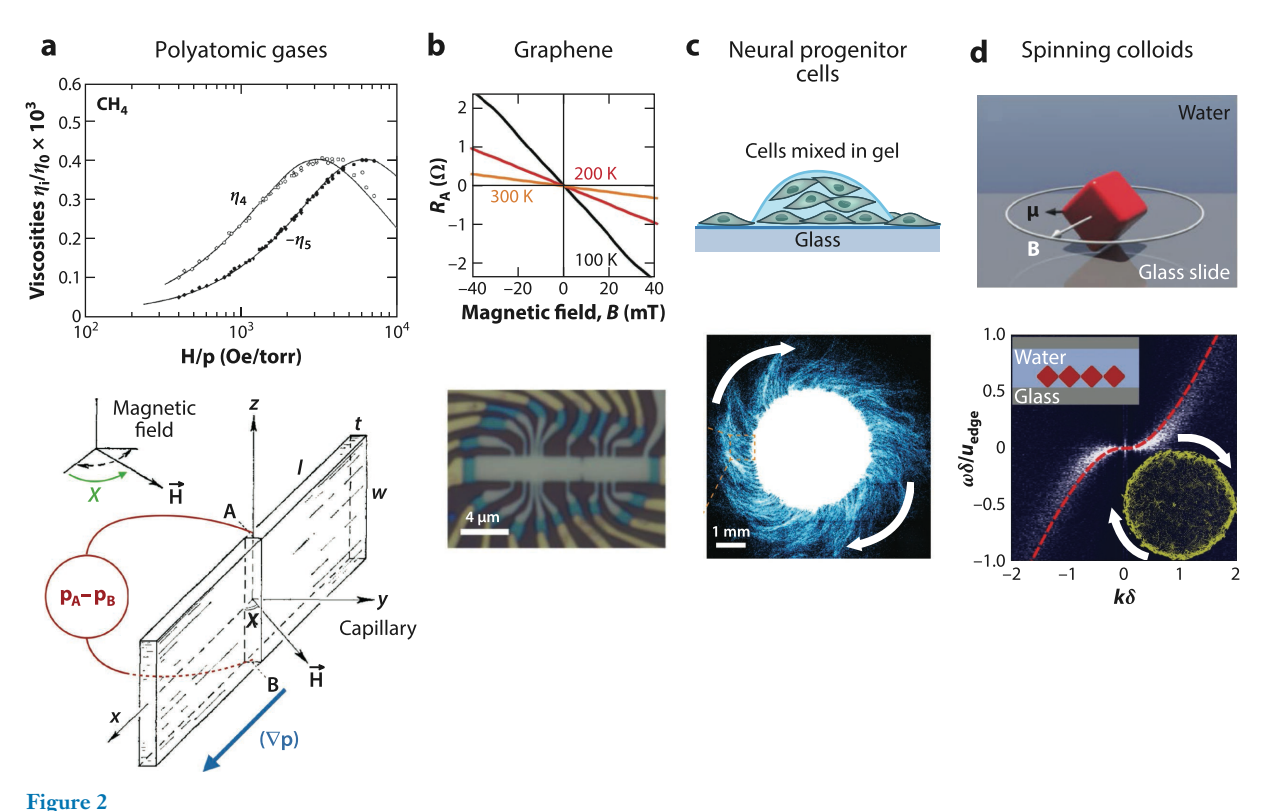


Figure 2

Experimental platforms for odd viscosity. (a) Three-dimensional magnetized polyatomic gases such as N₂, CO, or CH₄ exhibit odd viscosities (called η_4 and η_5 in the nomenclature of Reference 11). When the gas flows in a capillary, odd viscosity can be measured via the transverse pressure it creates. As an example, the odd viscosities of CH₄ are plotted as a function of H/p, where H is the external magnetic field, p is the overall pressure, and η_0 is the viscosity of the gas with no magnetic field. Panel adapted from Reference 38. (b) A 2D fluid of electrons in graphene under a magnetic field exhibits an odd shear viscosity (Hall viscosity), which can be determined from multiterminal electric transport measurements. Panel adapted with permission from Reference 88, AAAS. (c) It has been suggested that the flow of in vitro neural progenitor cells can exhibit odd viscosity. Panel adapted from Reference 92. (d) A 2D fluid consisting of small cubes with a permanent magnetic dipole moment in a colloidal suspension under a rotating magnetic field exhibits odd viscosity. It can be measured from the decay of surface waves originating from the antisymmetric part of the stress. Panel adapted with permission from Reference 52; copyright 2019 Springer.

to induce density changes implied by $\delta\rho \propto \delta p = -\eta^\circ \omega$ (30). For example, a Lamb–Oseen vortex without odd viscosity exhibits a density dip due to inertia. This dip can either be deepened or changed into a peak depending on the relative signs of odd viscosity and vorticity (30). In addition, correlations between density and vorticity due to odd viscosity are expected to occur at the level of fluctuating hydrodynamics (39). In strongly compressible flows, odd viscosity can also lead to transverse flows under the influence of the term $\eta^\circ \epsilon \cdot \Delta v$ in Equation 11, which is rotated by 90° with respect to Δv . This occurs, for instance, in compression shocks (6, 30), as illustrated in **Figure 1***b*, in which a flow develops transverse to the direction of travel of the shock.

2.2.3. Boundary effects. Odd viscosity has an effect on the flow even in incompressible 2D fluids when boundary conditions involve the stress.⁷ For instance, surface waves have been used

⁷What boundary conditions are appropriate to describe a certain system is a complex question even in passive fluids (32, 45). Although microscopic considerations provide some guidance, the answer ultimately boils down

to measure odd viscosity in a colloidal chiral fluid made of spinning magnetic cubes (52); see Section 2.4.5. In these experiments, the antisymmetric part of the stress tensor (see the sidebar titled Antisymmetric Stress), corresponding to the terms τ and η^R in Equation 9, produces chiral surface waves on top of a persistent particle current at the edge. Although not responsible for the presence of these surface waves, odd viscosity modifies their dispersion relation and damping rate in a way that can be measured.

In systems without antisymmetric stress, odd viscosity induces distinct chiral surface waves with dispersion $\Omega \approx -2\nu^{\circ}q|q|$ at a free surface (with a no-stress boundary condition), in which $\nu^{\circ} = \eta^{\circ}/\rho$ (53–55). Another class of boundary effects are topological sound waves (40, 56, 57). These occur in compressible odd viscous flows under the combined influence of the Lorentz (or Coriolis) body force and odd viscosity. We refer to References 58 and 59 for a pedagogical introduction to topological waves; the gist is that these topological waves are unidirectional sound waves appearing at the boundary of the fluid because it has to untangle its internal topology (**Figure 1***a*). Here, odd viscosity provides a short-distance cutoff that makes the topological invariant well defined and triggers unusual topological phase transitions (40, 56).

Finally, the drag and lift forces on an object embedded in a 2D fluid with odd (shear) viscosity have been analyzed in References 31, 44 and 60–62. The total lift force on a fixed object in a 2D incompressible fluid is not changed by η° , although the contributions to the lift force from pressure and shear stress are both modified (31). However, a change in the lift force has been reported in compressible odd fluids (62).

2.2.4. Low Reynolds number limit: Stokes flows. In the limit of low Reynolds numbers, the term $v \cdot \nabla v$ can be ignored in the Navier–Stokes Equation 5, which reduces to the so-called Stokes equation. Because the Stokes equation is linear, the general solutions are expressed in terms of its Green function $G_{ij}(x)$, called the Oseen tensor, which gives the flow in response to a point force (63, 64). In normal fluids, there is a symmetry in the exchange between the source (that produces a force) and the receiver (that measures the velocity field) called Lorentz reciprocity, which is expressed by $G_{ij} = G_{ji}$ (65, their section 4.2, equation 4.7). In fluids with odd viscosity, $G_{ij}(x) \neq G_{ij}(x)$, so Lorentz reciprocity is broken (4, 66).

In Reference 61, swimming in a 2D fluid with odd (shear) viscosity is analyzed. The fluid produces a torque on the swimmer when it changes area. In 3D Stokes flow, odd viscosity can no longer be absorbed in the pressure, even if the fluid is incompressible, leading to azimuthal flows that would otherwise be absent (4). This is illustrated in the flow past a sphere in **Figure 1d**, where an azimuthal velocity appears with opposite sign above and below the sphere.

2.2.5. Hydrodynamic instabilities. Hydrodynamic instabilities are abrupt changes in a fluid flow that arise when a control parameter is varied (67). How does odd viscosity affect these instabilities?

Let us first ask a simple question: Is an odd viscous fluid at rest linearly stable? It turns out that the answer is determined solely by the dissipative viscosities. To see that, let us linearize Equation 5

to whether the continuum theory correctly describes the experimental system under consideration (32, 45–49). For example, in a gas of rotating dumbbells (50, 51), a solid boundary prevents the rotation of the particles, leading to a boundary flow ($\mathbf{v} = \mathbf{v}_0 \neq \mathbf{0}$) rather than a no-slip condition. Similarly, frictional rotating disks roll without slipping on solid boundaries, leading again to a net flow and a nonzero hydrodynamic slip velocity. ⁸The dimensionless Reynolds number $Re = \rho U L / \eta$, where U is a characteristic velocity and L is a characteristic length, measures the ratio between inertial and viscous forces. In some situations, it can be helpful to define by analogy an odd Reynolds number $Re^o = \rho U L / \eta^o$ (see, for instance, References 30 and 40).

Onsager-Casimir reciprocity: symmetry between the matrices of transport coefficients at opposite values of the time-reversal breaking field *B* (rotation, magnetic field, etc.)

Green-Kubo relation: a formula relating the fluctuations of a system at rest and its response to a finite perturbation and Equation 6 about the state $\mathbf{v} = \mathbf{0}$ with a uniform density ρ , yielding $\rho \partial_t v_i = -\eta_{ijk\ell} q_j q_\ell v_k$. Multiplying by v_i , we find

$$\rho \partial_t \left(\frac{\|\boldsymbol{v}\|^2}{2} \right) = -\eta_{ijk\ell} q_j q_\ell v_k v_i = -\eta_{ijk\ell}^S q_j q_\ell v_k v_i,$$
 16.

in which the odd viscosities drop out in a way similar to that in Equation 7. In particular, if the symmetric part of the matrices of viscosities is positive-definite, the fluid is linearly stable.⁹

The effect of odd viscosity can be more dramatic in more complex flows, in which it can lead to both destabilization and stabilization. For instance, the magnetized Kelvin–Helmholtz instability (in magnetohydrodynamics) is modified by the presence of odd viscosities and is either stabilized or destabilized depending on the sign of the odd viscosity coefficient (68–70). Odd viscosity also prevents the breakup of clouds of sedimenting particles (4) in an odd viscous fluid (see **Figure 1***g*), and stabilizes the Saffman–Taylor instability (41). Further examples have been studied in falling thin films (71–75) and in plasmas (76–78; more references in Section 2.4.2).

2.3. Statistical Thermodynamics of Odd Viscosity

The viscosity tensor represents the diffusive transport of momentum. Near equilibrium, the theory of transport processes is structured around two concepts (11, 79, 80): The Green–Kubo relations provide a link between transport coefficients and fluctuations at equilibrium; and the Onsager–Casimir reciprocity relations provide algebraic constraints on transport coefficients. Neither of these principles are guaranteed in general far from equilibrium, raising the question, To what extent do they apply to odd viscosity?

2.3.1. Green–Kubo relations. In fluctuating hydrodynamics, the stress tensor fluctuates about its mean value. These fluctuations are characterized by the time correlation functions $\langle \sigma_{ij}(t)\sigma_{k\ell}(0)\rangle$ (we ignore spatial fluctuations for simplicity). When the correlations are symmetric in time, i.e., when

$$\langle \sigma_{ij}(t)\sigma_{k\ell}(0)\rangle = \langle \sigma_{k\ell}(t)\sigma_{ij}(0)\rangle,$$
 17.

then we say that the system obeys detailed balance or microscopic reversibility. At equilibrium, the Green–Kubo relation states that the viscosities can be expressed in terms of these correlation functions as

$$\eta_{ijk\ell} = \frac{\mathcal{A}}{k_{\rm B}T} \int_0^\infty \left\langle \sigma_{ij}(t)\sigma_{k\ell}(0) \right\rangle \mathrm{d}t,$$
18.

in which \mathcal{A} is the area (or volume in three dimensions) of the system. Fluids with odd viscosity can exhibit the same relation (6, 15, 81, 82). In particular, inspection of Equations 17 and 18 reveals that odd viscosity arises when the correlation functions are not symmetric in time, namely when

$$\langle \sigma_{ij}(t)\sigma_{k\ell}(0)\rangle \neq \langle \sigma_{k\ell}(t)\sigma_{ij}(0)\rangle.$$
 19.

Green–Kubo relations have been used to describe the viscosity of quantum Hall fluids and other solid-state systems (83–85). In the context of active fluids, these relations were derived using the Mori–Zwanzig projection operator formalism and verified using molecular dynamics simulations in Reference 6 for the shear part of the viscosity tensor of a 2D active fluid, in which time-antisymmetric parts of the correlation functions have indeed been observed. They can also be

⁹Formally, the case of odd elasticity with an overdamped dynamics is identical (see Section 3.2.3).

obtained from the Onsager regression hypothesis (81, 82), as well as from kinetic theory (15). Examples from molecular dynamics simulations are discussed in Section 3.5.4 and figure therein). We emphasize, however, that the validity of Green–Kubo relations is a priori not guaranteed in nonequilibrium systems.

2.3.2. Onsager–Casimir reciprocity. The Onsager–Casimir reciprocity relations are constraints on transport coefficients, usually associated with microscopic reversibility (11, 86, 87). For the viscosity tensor, the Onsager–Casimir relations are expressed as

$$\eta_{ijk\ell}(\mathbf{B}) = \eta_{k\ell ij}(-\mathbf{B}),$$
20.

in which B symbolizes all external sources of time-reversal breaking (such as magnetic fields or rotation). The Onsager relations are a particular case of Equation 20, where the left- and right-hand sides describe the same system, so $\eta_{ijk\ell} = \eta_{k\ell ij}$. Using the shear viscosities in isotropic 2D systems in Equation 9 as an example, Equation 20 corresponds to $\eta(B) = \eta(-B)$ and $\eta^{\circ}(B) = -\eta^{\circ}(-B)$. When the matrix in Equation 9 is not symmetric, Onsager reciprocity is said to be violated. This occurs whenever $\eta^{\circ} \neq 0$. For all systems known to the authors, Onsager–Casimir reciprocity appears to hold: The antisymmetric component of the viscosity tensor changes sign under time-reversal, whereas the symmetric component remains unchanged.

However, the range of applicability of the relation in Equation 20 has not yet been fully delineated. Current numerical (6, 82) and experimental (88) results for the shear viscosities η and η° are in agreement with Equation 20, which is also compatible with theoretical results from nonequilibrium thermodynamics (10, 11) and from kinetic theory (15, 89–91). However, theoretical arguments based on the Onsager regression hypothesis (81, 82) suggest that nondissipative (odd) viscosities can exist in systems that do not break time-reversal symmetry at the level of stress correlations. In addition, the fact that the breaking of mirror symmetry and time-reversal invariance originate in the same physical phenomena in these systems can be a confounding factor, as both symmetries impose constraints on the transport coefficients.

2.4. Where to Find Odd Viscosity?

According to the "central dogma" of phenomenology, anything that is not forbidden will, in principle, be present. Odd viscosity can only occur when certain spatial (see Sections 2.1.1 and 2.1.2) and nonspatial (see Section 2.3.2) symmetries are broken. For example, the shear odd viscosity $\eta^{\rm o}$ can only exist if the fluid violates mirror symmetry. Below, we discuss some systems that exhibit odd viscosity. In practice, all experimental systems we are aware of break time-reversal symmetry and mirror symmetry and involve either spinning particles or an external magnetic field.

2.4.1. Polyatomic gases under magnetic field. Rarefied polyatomic gases (such as N_2 or CO) under a magnetic field exhibit odd viscosities (often called transverse viscosities in this context; 33–37), as well as transverse nondissipative thermal conductivities (see the sidebar titled Other Oddities). This is illustrated in **Figure 2a**. These effects have been experimentally observed in a variety of gases; see References 33 and 34 for extensive reviews (in particular, table 2 in Reference 33 and table 7.1 in Reference 34 for lists of the various measurements known at the time). Odd viscosities in these systems originate from the precession of the magnetic moment of

Onsager reciprocity: symmetry of the matrix of transport coefficients

¹⁰When the Green–Kubo relations discussed in Section 2.3.1 apply, the Onsager relations arise as a consequence of detailed balance (Equation 17). In the simplified kinetic theory discussed in Section 2.5.2, the Onsager–Casimir relations can be obtained from Equation 22 by assuming that $L(B) = L^{\dagger}(-B)$ (this relation may then be derived from microscopic considerations in a given system).

OTHER ODDITIES

Odd responses similar to odd viscosity or elasticity arise in various contexts and are often associated with a transverse response (93). Perhaps the most well known is the Hall effect: a transverse voltage difference arises in response to a longitudinal electric current in electric conductors under magnetic field. This originates from the local Ohm law $j = \sigma E$ relating the current density to the electric field, in which the electrical conductivity σ acquires an antisymmetric part called Hall conductivity. Similar phenomena arise in heat diffusion (under the names of thermal Hall or Righi–Leduc effects; 94), in particle diffusion (see References 95–98, and references therein), in light diffusion (99, 100), or in the case of Willis couplings (101). See Reference 93 for a review of Hall-like effects. Analogs of odd elasticity also occur in the generalized elasticity (102, 103) of mesophases with nonvariational dynamics such as active cholesterics and hexatics (104, 105). As an example, consider the diffusion equation

$$\partial_t \rho + \nabla \cdot \mathbf{j} = 0$$
 where $\mathbf{j} = -\mathbf{D} \nabla \rho$,

in which ρ is the particle density. The antisymmetric part of the diffusion tensor D_{ij} contains odd (Hall) diffusivities. In a uniform system, $\nabla \cdot \mathbf{j} = D_{ij}\partial_i\partial_j\rho$, so odd diffusivities drop out of the equation of motion. They can still be observed if they enter the boundary conditions or if the current can be measured directly.

the molecules due to the external magnetic field, which modifies the collision cross-section of the molecules. These experimental studies are part of a large body of work on the effect of electric and magnetic fields on transport properties, which occurred hand in hand with progress made in kinetic theory (33, 34). The measurement of transverse viscosities has also been used to determine the sign of the so-called *g*-factor of the molecules (a dimensionless proportionality constant relating the magnetic moment and the angular momentum of an object; 106).

2.4.2. Magnetized plasma. Electrically conducting fluids such as plasma or liquid metals can directly couple to a magnetic field (externally produced or induced by the fluid motion). These systems are described by a continuum theory called magnetohydrodynamics (MHD), in which the coupled dynamics of the fluid density ρ , its velocity field v, and the magnetic field B are described. In a magnetized plasma, time-reversal symmetry and parity (mirror symmetry) are broken, so we expect odd viscosities to arise, and indeed they do. As reviewed in Sections 2.5.1 and 2.5.3, the physical mechanism relies on the fact that charged particles in a magnetic field have a tendency to rotate along circular orbits because of the Lorentz force. In this context, odd viscosity is usually known as gyroviscosity.

The existence of gyroviscosity has been established from kinetic theory calculations (107–110) as well as from more heuristic approaches (77, 111). Consequences of gyroviscosity have been explored in the context of magnetic confinement fusion (112; in particular, their section III.D.2, and references therein), and in the context of the ionosphere and magnetosphere of planets (68, 113, and references therein). Gyroviscosity is expected to stabilize certain instabilities that would otherwise occur and to destabilize otherwise stable situations, in qualitative agreement with experimental observations (70, 76–78, 112, 114–125). As an example, gyroviscous theories have been used to model the observed dusk–dawn asymmetry in the Kelvin–Helmholtz instabilities occurring in the magnetosphere of planets (68, 70, 116).

2.4.3. Gases under rotation. Odd viscosity is expected to arise in gases under rotation as a consequence of Coriolis forces. This prediction has been made using kinetic theory in dilute gases (126), and we sketch the physical mechanism in Section 2.5.1. One finds that the ratio of odd over normal viscosity is given by $\eta^{\circ}/\eta \sim \Omega \tau$, where Ω is the angular frequency of rotation and

Gyroviscosity: synonym of odd viscosity in the context of plasma physics

 $\tau \sim \eta/p$ is a collision time, expressed in terms of the shear viscosity of the unperturbed fluid η and the pressure p. This estimate suggests that obtaining a sizeable odd viscous response would require a combination of low pressures, high viscosities, and fast rotation. To give an order of magnitude, in order to have $\eta^{\circ} \sim \eta$, the required spinning speed should be of the order of $\tau^{-1} \simeq 1 \times 10^{9} \, \mathrm{s}^{-1}$ for air at atmospheric pressure.

2.4.4. Condensed matter: graphene, superfluids, etc. The transport of electrons in a metal is usually described by Ohm's law, but this is not the only possibility (49, 127–133). When only electron–electron collisions occur, electrons behave like a viscous fluid. This has been observed in high-mobility systems such as graphene (127–132). In this regime, odd viscosities (called Hall viscosities in this context) occur when the electrons are put in a magnetic field, so time-reversal symmetry is broken. Hall viscosities lead to corrections to charge transport quantities such as resistances. An isotropic 2D shear Hall viscosity has been measured in graphene under magnetic field from transport measurement in multiterminal Hall bars (88), where the normal shear viscosity is $\nu \approx 20 \times 10^{-2} \text{ m}^2/\text{s}$ at $T \approx 100 \text{ K}$, whereas $\nu^o \approx 7 \times 10^{-2} \text{ m}^2/\text{s}$ at $B \sim 40 \text{ mT}$. Here, $\nu = \eta/\rho$ and $\nu^o = \eta^o/\rho$.

Odd viscosity is also expected in superfluids under magnetic field or under rotation such as liquid helium and other chiral superfluids (84, 134–138). In gapped quantum Hall fluids, odd viscosity contains information about the topological order of the state (5, 43, 83, 85, 138–143). In this case, in a rotationally invariant 2D system, the Hall viscosity is proportional to a quantized topological invariant S called shift through $\eta^{\circ} = \hbar(S/4)n$, where \hbar is the Planck constant and n is the electron density.

2.4.5. Active and driven soft matter. Fluids composed of active objects exhibiting a preferred chirality are called chiral active fluids (6, 30, 51, 144–147). They include collections of self-spinning colloidal particles (52, 147–149), circle swimmers (150, 151), driven chiral grains (50), and 3D-printed rotors fluidized by a turbulent upflow (98, 152), as well as robotic systems (153, 154) and biological matter (92, 155–157). Theoretical works have predicted that these systems exhibit odd viscosity as well as hydrostatic torques (see the sidebar titled Antisymmetric Stress) (30, 144, 150, 151, 158).

Experimental measurements of odd viscosity have been performed in a fluid made of spinning colloids (52). The colloidal cubes suspended in water over a glass surface have a magnetic moment and spin under the effect of a rotating magnetic field. Odd viscosity is then measured through modifications in the dispersion of surface waves (see Section 2.2.3), and the values reported are $\eta^{\circ} = (1.5 \pm 0.1) \times 10^{-8}$ Pa ms and $\eta = (4.9 \pm 0.2) \times 10^{-8}$ Pa ms.

Odd viscosity has also been numerically observed in simulations of dense but passive chiral fluids composed of ratchet-shaped particles in simple shear and planar extensional flows (24, 159; see also 160). Magnetized nematic ferrofluids are also expected to exhibit odd viscosities (19, 20).

2.4.6. Vortex matter. In an ideal fluid, stable point vortices can exist and interact with each other. A large collection of such vortices can itself be treated as a fluid. It has been predicted that such a 2D fluid composed of vortices of the same sign exhibits odd viscosity (161–163). Intuitively, this can be understood from the fact that the vortices have transverse interactions (breaking the symmetries that would forbid odd viscosity in two dimensions). It has also been reported that numerical simulations of skyrmions in chiral magnets exhibit odd viscosity (164).

¹¹The diffusive behavior described by Ohm's law arises when only electron–lattice collisions are present. When all collisions are negligible, the transport is ballistic. When both electron–electron and electron–lattice collisions are present, the behavior of electrons is similar to the flow of a viscous fluid in a porous medium (127).

2.5. Microscopic Mechanisms

Microscopically, odd viscosity can arise from at least two classes of mechanisms: (a) as a single-particle effect originating from an individual particle's dynamics between collisions (this is discussed in Section 2.5.1) and (b) as an effect of interactions between particles (Section 2.5.2). We first discuss the physical mechanisms and then outline how continuum equations can be obtained from microscopics using kinetic theory (Section 2.5.3). Finally, we sketch how odd viscosity can be obtained from variational principles consistent with microscopic symmetries (Section 2.5.4).

2.5.1. Collisionless odd viscosity. Odd viscosity can be generated by the individual motions of particles in an external field. The Lorentz force (for charged particles in a magnetic field) and Coriolis force (for all particles in a rotating reference frame) tend to move the particles along circular orbits. This single-particle effect leads to odd viscosity. To illustrate how this works, consider a gas of charged particles in an external magnetic field, as shown in Figure 3. Recall that an individual charged particle in a magnetic field follows a circular orbit called a Larmor orbit or cyclotron orbit, whose center is called the guiding center and radius is called the Larmor radius (see References 165 and 166 for more about plasma physics). When the Larmor radius is small enough (in a thermal plasma, this occurs at large enough magnetic field), the gyrating particle behaves as a magnetic point dipole aligned with the field and located at the guiding center.

The guiding center of the particles in the plasma can move under the influence of external forces and of other particles. For a collection of particles, this motion is summarized by the velocity field of the plasma. In a nonuniform external force (such as an electric field), the cyclotron orbit of a single particle deforms into an ellipse. This can be shown explicitly from the equations of motion for a single particle (77, 111; see also the **Supplemental Text**). At the continuum level, the nonuniform external force leads to a velocity gradient. As illustrated in **Figure 3**, the elliptic cyclotron orbit is rotated by 45° with respect to the velocity gradient. The resulting momentum flux is therefore also rotated by 45°. This means that a shear rate 1 (\dot{e}_2) in **Table 1** leads to minus a shear stress 2 ($-\sigma_3$), whereas a shear rate 2 (\dot{e}_3) leads to shear stress 1 (σ_2): This corresponds to

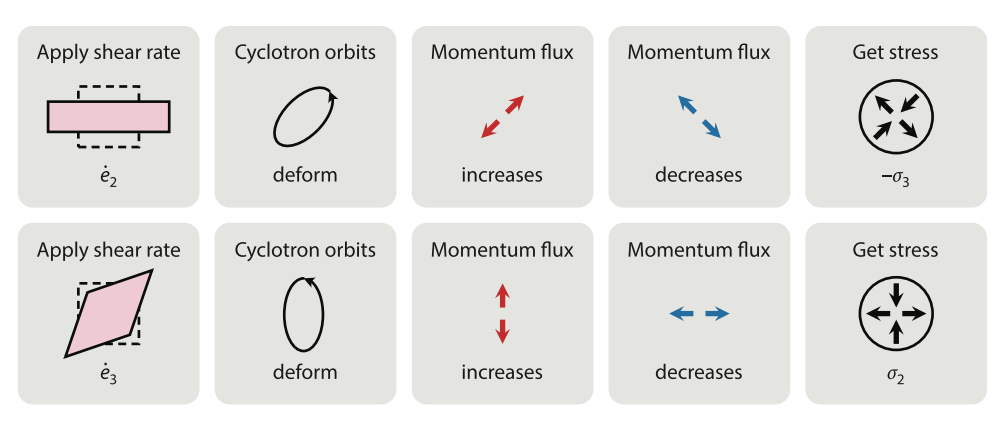


Figure 3

Collisionless odd viscosity. In a magnetized plasma, the charged particles follow closed trajectories called cyclotron orbits. In a fluid at rest, the orbits are circular. When a shear rate (in the plane orthogonal to the magnetic field) is applied to the fluid, the cyclotron orbits become elliptic. The principal axes of the ellipse are rotated by 45° with respect to the shear rate axes with a handedness set by the magnetic field. This leads to a stress rotated by 45° from the shear rate, corresponding to odd viscosity.

the odd shear viscosity η° in Equation 9. Hence, odd viscosity is due to the deformation of the Larmor orbits. Because the mechanism goes beyond the picture of effective dipoles, it is known as a finite Larmor radius effect or as a nonideal MHD effect. This effect can be captured in a more systematic manner using kinetic theory (77, 107–109, 111).

2.5.2. Odd viscosity from collisions. The preceding section discussed a mechanism in which odd viscosity is essentially a single-body effect: the free trajectory of a particle is modified in between collisions. However, odd viscosity can also arise as the result of abnormal collisions, even when the free motion of particles is unchanged. In typical fluids, the collisions are, on average, invariant under mirror reflections (**Figure 4***a*,*b*). In contrast, collisions that on average violate parity (i.e., mirror reflection symmetry, as in **Figure 4***c*,*d*; 50, 52, 149) can lead to odd viscosity (6, 15). The mechanism can be understood pictorially (**Figure 4**). When we subject the fluid to a constant shear rate (shown in **Figure 4***e*), vertical collisions are more frequent and horizontal collisions are less frequent than in the fluid at rest. The resulting change in the momentum flux is qualitatively obtained by examining where particles go after collision. When the collisions are asymmetric (**Figure 4***d*), there is an increase of the momentum flux at 45° and a decrease of the

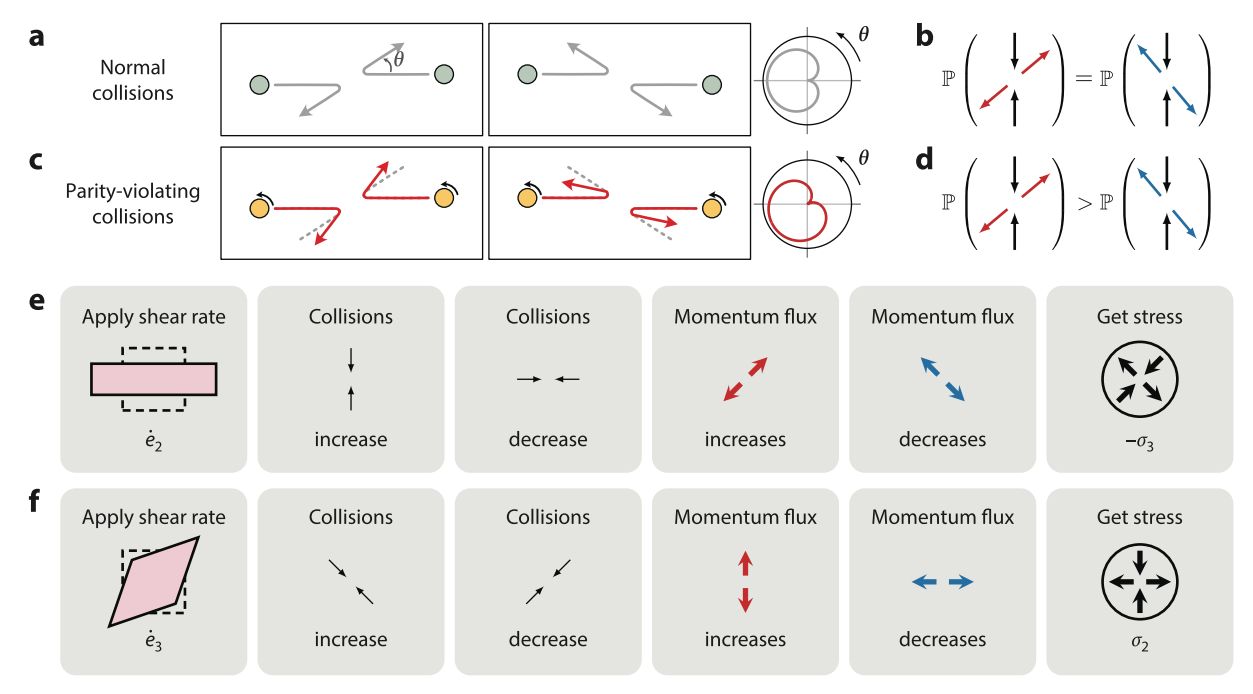


Figure 4

Odd viscosity from collisions. (a,b) In the case of normal collisions, the cross-section $\sigma(g,\theta)$ giving the probability of particles going out with an angle θ is symmetric: $\sigma(g,\theta) = \sigma(g,-\theta)$, where g is the center of mass momentum. (c,d) This is not the case for parity-violating collisions, for which $\sigma(g,\theta) \neq \sigma(g,-\theta)$. (e) The fluid is subjected to a constant shear rate \dot{e}_2 (see **Table 1**). As a consequence, there are more vertical collisions and fewer horizontal collisions compared to the fluid at rest. The change in the momentum flux (compared to the fluid at rest) is qualitatively obtained by looking at where particles go after collision. As the collisions are asymmetric (see panel d), there is an increase of the momentum flux at 45° (in red) and a decrease of the momentum flux at -45° (in blue). Combining these, we find the resulting viscous stress $-\sigma_3$ in the rightmost part of panel e. Note that the momentum flux tensor (pressure tensor) is the opposite of the stress tensor. There are also changes in the horizontal and vertical momentum fluxes, which correspond to normal shear viscosity and are not shown. (f) We follow the same reasoning as that in panel e when the fluid is subjected to a constant shear rate \dot{e}_3 . The result is a viscous stress σ_2 . Hence, we have found that $\sigma_2 \propto \dot{e}_3$ and $\sigma_3 \propto -\dot{e}_2$ (ignoring normal shear viscosity), which is the effect of odd viscosity. Figure adapted from Reference 15.

momentum flux at -45° . The corresponding viscous stress is the opposite of this momentum flux. Repeating this argument for a constant shear rate at 45° (**Figure 4***f*), we find an increase in the vertical momentum flux and a decrease in the horizontal momentum flux. The relations between the resulting stresses and the strain rates we apply in **Figure 4***e* and **Figure 4***f* are antisymmetric: This is odd viscosity.

Realistic microscopic descriptions of magnetized neutral polyatomic gases, which take into account internal molecular degrees of freedom, indeed agree quantitatively with measured nondissipative transport coefficients (33–37, 167–176). The main ideas from these calculations can be captured via a simplified model in which the internal degrees of freedom are neglected and only the fact that collisions are not invariant under mirror symmetry are kept (15).

2.5.3. Kinetic theory. In this section, we sketch how (odd) viscosities can be obtained from microscopic models using kinetic theory. We focus on the simplest case, and refer the reader to the literature (33–37, 167–176) for more realistic cases. To do so, let us consider the distribution function f(t, r, c), giving the probability $f(t, r, c) d^d r d^d c$ of finding a particle in a volume centered at position r and velocity c in phase space at time t. The fluid at rest is described by a stationary distribution such as the Boltzmann distribution $f^{\circ} \propto \exp[m\|c - v\|^2/(2k_BT)]$ (v is the fluid velocity, T is the temperature, m is the particles' mass, and k_B is the Boltzmann constant). Viscosity is contained in the way the distribution function relaxes toward equilibrium after being perturbed by a velocity gradient. This relaxation can be described by kinetic theories, such as the Boltzmann equation. When linearized about the stationary distribution, the Boltzmann equation reads as (107, 177, 178)

$$\frac{\partial \phi}{\partial t} + c_i \frac{\partial \phi}{\partial r_i} + b_i \frac{\partial \phi}{\partial c_i} = L\phi,$$
21.

where $f = f^{\circ}(1 + \phi)$, $m\mathbf{b}$ are body forces, and L is the linearized collision operator. L can be expressed in terms of the scattering cross-section $\sigma(g, \theta)$ defined in **Figure 4**. Equation 21 expresses the conservation of probability, where the left-hand side captures the probability flow without interactions and L on the right-hand side captures the redistribution of probability due to collisions.

Let us first consider the case of chiral collisions with no external force (b = 0). The viscosity tensor can be expressed as an inner product of the form (15)

$$\frac{\eta_{ijk\ell}}{\rho} = -\frac{m}{k_{\rm B}T} \left(c_i c_j, L^{-1} c_k c_\ell \right), \qquad 22.$$

where $(\chi_1, \chi_2) = (m/\rho) \int f^{\circ}(c) \overline{\chi_1(c)} \chi_2(c) d^d c$. An explicit calculation shows that when collisions are chiral $[\sigma(g, \theta) \neq \sigma(g, -\theta)]$, the linearized collision operator L becomes non-Hermitian $(L \neq L^{\dagger})$, which leads to odd viscosity $\eta_{ijk\ell} \neq \eta_{k\ell ij}$ through Equation 22.

The case of particles in a magnetic field (or in a rotating reference frame) can be treated in a similar way. The charged particles are subject to an out-of-plane magnetic field B and experience a Lorentz force, $mb_i(c) = m\omega_B\epsilon_{ij}c_j$, where $\omega_B = (q/m)B$ (q is the charge) or equivalently a Coriolis force on neutral particles in a frame of reference rotating at angular frequency $\Omega = \omega_B/2$. Here, the collisions are not chiral, so we can model them using the so-called relaxation time approximation, where $L\phi \simeq -\phi/\tau$ in Equation 21, in which τ is a relaxation time (177). The viscosity can then be obtained. A simplified calculation is given in Reference 111, which produces $\eta = p\tau/(1 + 4\tau^2\omega_B^2)$ and $\eta^\circ = 2\omega_B\tau\eta$. See References 107–109 and 126 for more detailed calculations.

2.5.4. Action principles and Hamiltonian structure. The dynamics of an ideal fluid can be obtained from an action or a Hamiltonian (179). The action of such an ideal fluid is

$$S = \int \left(\frac{1}{2}\rho \|\mathbf{v}\|^2 - \rho U\right) dt d^d r,$$
 23.

in which v is the velocity field, ρ is the density field, and U is the internal energy per unit mass of the fluid. Imposing a stationary action $\delta S = 0$ directly leads to the Euler equation. To be precise, the action in Equation 23 is written in Eulerian coordinates, but it must be varied in Lagrangian coordinates (179). From the action principle, one can deduce a Hamiltonian and a Poisson bracket structure as well. This point of view provides useful insights on conservation laws, the stability of the fluid, and approximation methods (179, 180).

Because odd viscosity does not contribute to dissipation, it is a form of ideal flow and can be captured in this framework. The main idea, originating in the physics of plasma (181–186) and recently analyzed in the context of active and electronic matter (30, 158, 187), consists of adding to the action a term

$$\Delta S = \int \mathbf{L} \cdot \boldsymbol{\omega} \, \mathrm{d}t \, \mathrm{d}^d r$$
 24.

in which $\omega = \nabla \times v$ is the vorticity, and L is a new quantity introduced phenomenologically, which sometimes corresponds to the density of angular momentum.

In the context of gapped quantum Hall fluids, odd viscosity has also been described by so-called topological terms known as the Wen–Zee and (gravitational) Chern–Simons actions (139, 143, 188–191). In the case of gapless fluids, it has been described by another kind of topological term known as the Wess–Zumino–Witten action (192; see also 26, 193 for other effective field theory approaches).

3. ODD ELASTICITY

The canonical formulation of elasticity typically assumes that the stress–strain relationship is compatible with a potential energy. This assumption is in general not appropriate for a range of living, driven, or active media, and odd elasticity is the theory that emerges when this assumption is removed.

3.1. What Is Elasticity?

When you gently deform a solid, such as a rubber pencil eraser, the solid resists the shape change you are trying to impart. This is due to elasticity, which captures the resistance of a solid against inhomogeneities in its displacement field. The elastic solid exerts stresses,

$$\sigma_{ii} = C_{iik\ell} \partial_{\ell} u_k, \qquad 25.$$

in response to shape changes, described by gradients $e_{k\ell} = \partial_\ell u_k$ of the displacement field u(t, x). The stress tensor describes the forces that a parcel of elastic continuum applies to the neighboring parcels, or to the environment. The coefficient of proportionality $C_{ijk\ell}$ is called the elasticity tensor, also known as the elastic modulus tensor or stiffness tensor. Each independent component of $C_{ijk\ell}$ is referred to as an elastic modulus.

Let us consider a cyclic deformation in which we slowly deform an elastic solid so that it goes back to its original configuration when we are finished (as shown in **Figure 5**). The total work done (which is computed in Section 3.3) is then

$$\Delta W^{\text{el}} = \int \dot{W}^{\text{el}} dt = -\int dt \, d^d x \, C^{\text{A}}_{ijk\ell}(\partial_j \dot{u}_i)(\partial_\ell u_k), \qquad 26.$$

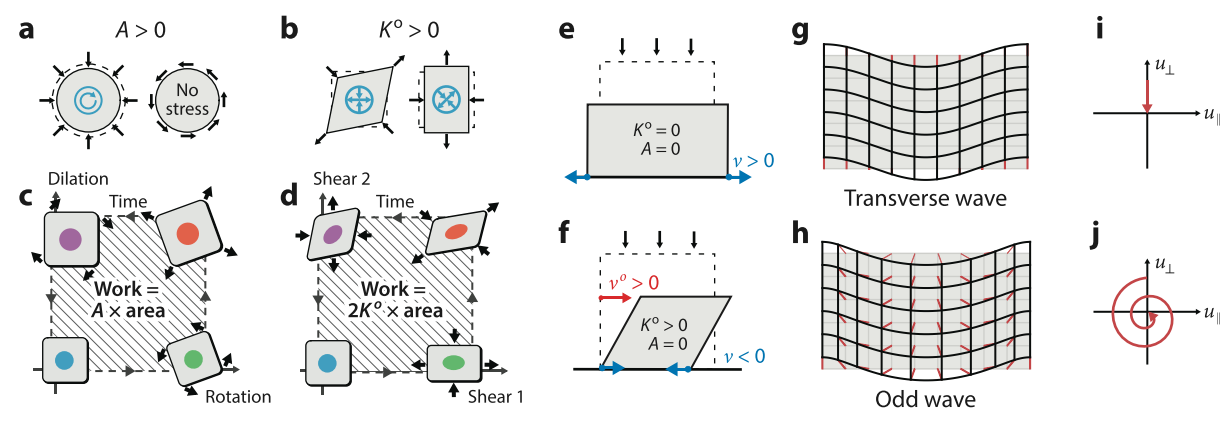


Figure 5

Odd elasticity. (a) The odd modulus A induces a torque density when the medium is dilated or compressed. (b) The odd modulus K° induces a shear stress that is rotated with respect to the applied shear strain. The black arrows are a proxy for deformation, and the blue arrows indicate the stress. (c,d) Both A and K° are nonconservative. This means that there exists (quasistatic) cycles of deformation along which the work done is nonzero. (e) A uniaxial compression of a passive material generically results in symmetric deformation. If the material sides move outward, its Poisson ratio ν is positive. (f) A uniaxial compression of an odd elastic block results in a tilt whose intensity is proportional to the odd ratio ν° . If K° is sufficiently large, the material also becomes auxetic (ν < 0), meaning that the material contracts in response to compression. (g) A transverse wave in a passive solid is illustrated. (b) An odd elastic wave propagates with a circular polarization. The thin red lines represent the displacement field. (i) For an overdamped passive solid, the displacement field of the transverse mode decays toward its rest position along a straight line. (j) For an overdamped odd elastic solid with $K^{\circ} > 0$, the displacement field traces out spirals that become closed ellipses when $B = \mu = 0$. Figure adapted with permission from Reference 194, copyright 2020 Springer Nature.

in which only the antisymmetric part,

$$C_{ijk\ell}^{A} = [C_{ijk\ell} - C_{k\ell ij}]/2$$
 (odd elastic tensor), 27.

of the elasticity tensor appears. As a consequence, the work performed by elastic forces over a cyclic deformation vanishes provided that the elastic tensor is symmetric ($C_{ijk\ell}^{\rm A}=0$). An elastic medium where $C_{ijk\ell}^{\rm A}\neq 0$ is called odd elastic: In such a system, the work of elastic forces depends on the path taken in deformation space. As a consequence, it is possible to both loose and gain energy from the medium (depending on whether the cycle of deformations is performed in a direction or in reverse). Hence, materials exhibiting odd elasticity are typically active or driven, in the sense that they must contain or have access to energy sources. Elasticity can also be used to model systems in which the stress σ is not physically a current of linear momentum, and $\Delta W^{\rm el}$ is therefore not an energy. In these cases, odd elastic moduli can arise without activity (see Sections 3.4.2–3.4.6).

3.2. Case Study: Two-Dimensional Isotropic Solids

To illustrate odd elasticity in a concrete setting, we ask the following: What does odd elasticity look like in a 2D isotropic solid? Besides providing a mathematically simple illustration of the general concepts (194), this setting is relevant for many of the experimental systems discussed in Section 3.4 and **Figure 6**. Examples of anisotropic and 3D odd elastic materials are discussed in Section 3.4.5 and References 194–196.

3.2.1. Two-dimensional odd elastic moduli. Because $C_{ijk\ell}$ is a rank 4 tensor, in two dimensions it has at most $2^4 = 16$ independent coefficients. However, assumptions such as spatial symmetries, coupling to rotations, and angular momentum conservation constrain the number of independent parameters. To enumerate the components of $C_{ijk\ell}$, we use the same basis for stress and strain as

Odd elastic modulus: an antisymmetric component of the elasticity tensor

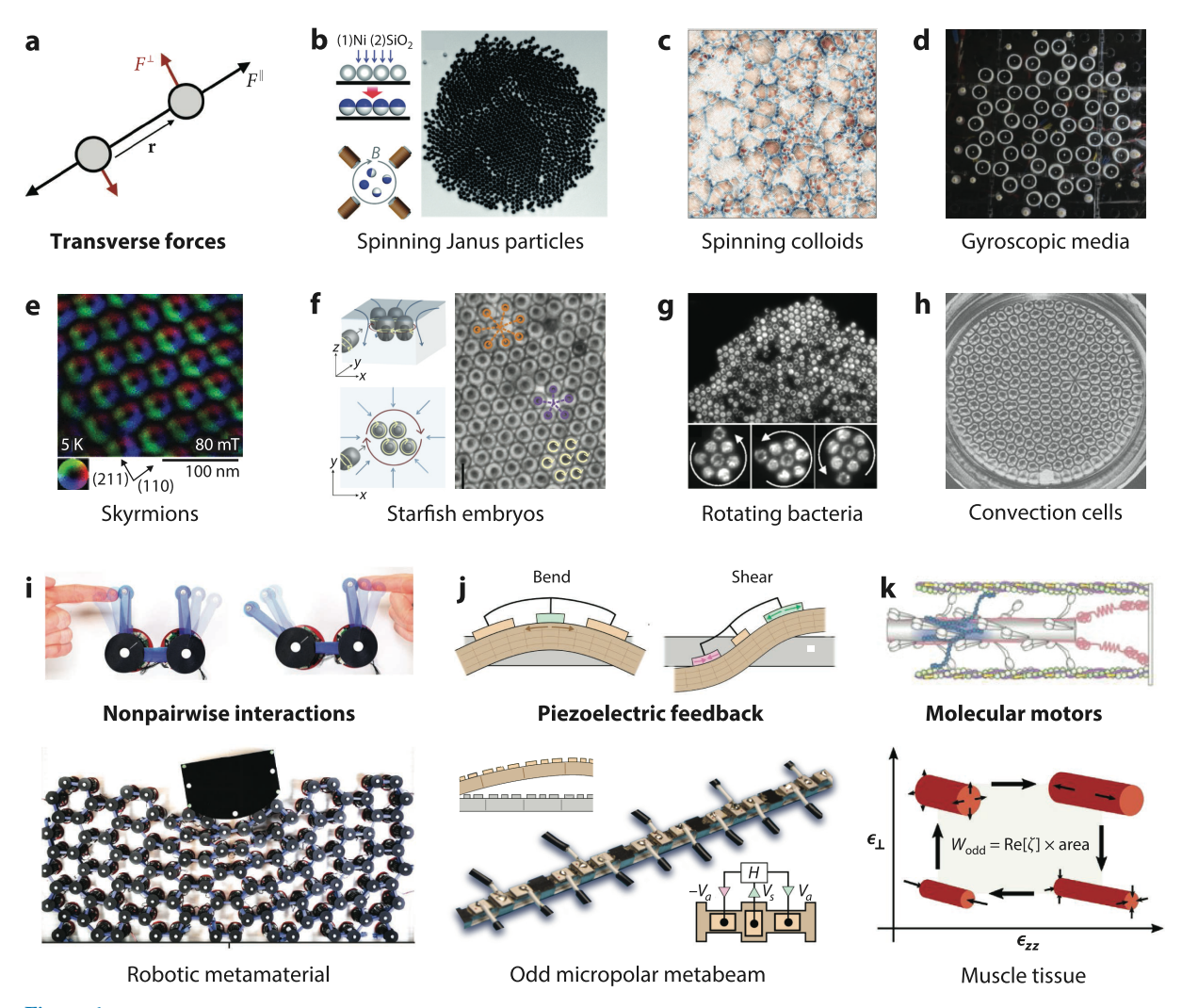


Figure 6

Experimental platforms for odd elasticity. (a) A pairwise interaction with a longitudinal force $F^{\parallel}(r)$ (black) and a transverse force $F^{\perp}(r)$ (red) connects two particles (circles). (b) Janus particles and (c) hematite colloids driven to spin by external magnetic fields. Panel b adapted with permission from Reference 149, copyright 2021 Springer Nature. (d) A network of gyroscopes connected by springs is a realization of gyroscopic matter, whose elastodynamics can be mapped onto odd elasticity in the limit of fast-spinning gyroscopes. Panel adapted from Reference 239. (e) Skyrmion lattices exhibit transverse interactions via a Magnus force. Panel adapted with permission from Reference 240; copyright 2016 Springer Nature. (f) Starfish embryos and (g) bacteria form chiral crystals with particle rotation driven by flagella and cilia, respectively. Panel f adapted with permission from Reference 157, copyright 2022 Nature. Panel g reproduced with permission from Reference 156; copyright 2015 American Physical Society. (b) Rayleigh–Bénard convection cells organized in a hexagonal pattern. When the system is put under rotation, odd elasticity can appear. Panel adapted from Reference 241. (i) A realization of the active hinge described by Equation 47. Such hinges are tiled into a 2D wall to create an odd elastic solid. Panel adapted from Reference 220. (j) A moderately thick beam with piezoelectric patches that couple bending and shearing degrees of freedom. The repeated unit cell gives rise to a 1D chain with odd elasticity. Panel adapted from Reference 219. (k) A schematic depicting a muscle fiber, roughly 1 μ m in length. When many fibers are in a bundle, the active stresses can couple transverse and longitudinal strains antisymmetrically. Panel adapted from Reference 196.

that for the viscosity tensor in Equation 9 and **Table 1**. Under the assumption of isotropy, the stress-strain relationship takes the form (see the **Supplemental Text**)

where $p^{(\text{pre})}$ and $\tau^{(\text{pre})}$ are, respectively, the pressure and torque density present in the undeformed state (they are so-called prestresses). In Equation 28, B and μ are, respectively, the usual bulk and shear moduli. The odd elastic moduli are the antisymmetric contributions to the matrix in Equation 28, namely K^{o} and $A-\Lambda$. In standard tensor notation, $C_{ijk\ell}$ reads as

$$C_{ijk\ell} = B\delta_{ij}\delta_{k\ell} - A\epsilon_{ij}\delta_{k\ell} - \Lambda\delta_{ij}\epsilon_{k\ell} + \Gamma\epsilon_{ij}\epsilon_{k\ell} + \mu(\delta_{i\ell}\delta_{jk} + \delta_{ik}\delta_{j\ell} - \delta_{ij}\delta_{k\ell}) + K^{o}(\epsilon_{ik}\delta_{j\ell} + \epsilon_{j\ell}\delta_{ik}).$$
29.

Often, one also assumes that solid-body rotations do not induce stresses and, hence, one sets $\Lambda = \Gamma = 0$. This assumption, sometimes called objectivity, is natural if the microscopic forces only depend on relative distances between points in the solid and not on the orientation of the solid in space. It can be violated, for instance, in the presence of a substrate (197, 198). The remaining off-diagonal elastic moduli are A and K° . As illustrated in **Figure 5**a,b, the modulus A converts dilation into torque, and the modulus K° converts shear strains to shear stresses with a rotation of principal axes. **Figure 5**c,d shows examples of deformation cycles that extract energy via the moduli A and K° , respectively.

3.2.2. Elastostatics. One immediate consequence of the presence of odd elastic moduli is that the static response of a solid changes when it is exposed to external loads and stresses. For example, **Figure 5***e*, *f* illustrates a solid under uniaxial compression (194). Without odd elasticity, a typical solid deforms with left–right symmetry (**Figure 5***e*). In contrast, a solid with nonzero $K^o \neq 0$ displays a horizontal deflection in a direction determined by the sign of K^o (**Figure 5***f*). The ratio of the horizontal to the vertical motion of the top surface is dubbed the odd ratio v^o . Additionally, the Poisson ratio v measures the ratio of horizontal expansion to vertical compression. Their physical meaning is illustrated in **Figure 5***e*, *f* and their values are given by

$$v^{o} = -\frac{\partial_{y} u_{x}}{\partial_{y} u_{y}} = \frac{BK^{o}}{\mu(B+\mu) + (K^{o})^{2}} \quad \text{and} \quad v = -\frac{\partial_{x} u_{x}}{\partial_{y} u_{y}} = \frac{\mu(B-\mu) - (K^{o})^{2}}{\mu(B+\mu) + (K^{o})^{2}}.$$

For sufficiently large K° , the material becomes auxetic, meaning that $\nu < 0$.

3.2.3. Elastodynamics. So far, our discussion of elasticity has not yet involved any equations of motion. For inertial systems, the dynamics of the displacement field can be described by

$$\rho \partial_x^2 u_i + \gamma \partial_x u_i = f_i = \partial_i \sigma_{ii},$$
 30.

where ρ is the mass density, and the term $\gamma \partial_t u_i$ represents friction on a lubricated substrate. Explicitly, the equations read as

$$\rho \partial_t^2 \boldsymbol{u} + \gamma \partial_t \boldsymbol{u} = (B - \Gamma) \nabla (\nabla \cdot \boldsymbol{u}) + (\mu + \Gamma) \Delta \boldsymbol{u} + (K^{\circ} + \Lambda) \boldsymbol{\epsilon} \cdot \Delta \boldsymbol{u} - (A + \Lambda) \boldsymbol{\epsilon} \cdot \nabla (\nabla \cdot \boldsymbol{u}).$$
 31.

 $^{^{12}}$ A seemingly similar effect can occur in passive anisotropic elastic media when the direction of compression is not aligned with the principal axis of stiffness. The distinction is that in **Figure 5**f, the odd elastic modulus K^{o} is compatible with isotropy and, hence, the resulting deflection occurs with the same handedness regardless of the orientation of the material being compressed.

In the rest of this paragraph, we set $\Lambda = 0$ and $\Gamma = 0$ without loss of generality.¹³ Because Equation 31 is linear, it supports plane wave solutions $u(x) = u e^{i(q \cdot x - \omega t)}$ with wave number q and frequency ω . As a matrix equation in terms of the longitudinal $u_{\parallel} = \hat{q} \cdot u$ and transverse $u_{\perp} = \hat{q} \times u$ components, Equation 31 reads as

$$-(\rho\omega^{2} + i\gamma\omega)\begin{bmatrix} u_{\parallel} \\ u_{\perp} \end{bmatrix} = -q^{2}\begin{bmatrix} B + \mu & K^{o} \\ -K^{o} + A & \mu \end{bmatrix}\begin{bmatrix} u_{\parallel} \\ u_{\perp} \end{bmatrix} = D\begin{bmatrix} u_{\parallel} \\ u_{\perp} \end{bmatrix}.$$
 32.

The matrix D in Equation 32, known as the dynamical matrix, relates forces to displacements. When $\gamma=0$ and $A=K^\circ=0$, we recover the two usual types of elastic waves: a longitudinal and a transverse mode, with dispersions $\omega=\pm q\sqrt{\frac{B+\mu}{\rho}}$ and $\omega=\pm q\sqrt{\frac{\mu}{\rho}}$, respectively. The transverse wave is illustrated in **Figure 5g**. In contrast, in an overdamped system ($\rho=0$ and $\gamma>0$) passive elastodynamics ($A=K^\circ=0$) becomes diffusive: $\omega=-\mathrm{i}q^2\frac{B+\mu}{\gamma}$ and $\omega=-\mathrm{i}q^2\frac{\mu}{\gamma}$. In our convention, a negative imaginary frequency implies that a wave is attenuated. In the case of an overdamped odd elastic solid with $A,K^\circ\neq0$, we obtain

$$\omega = -iq^2 \frac{B/2 + \mu \pm \sqrt{(B/2)^2 - K^{o}(K^{o} - A)}}{\gamma}.$$
33.

Notice that when $K^{\circ}(K^{\circ} - A) > (B/2)^2$, the frequency has a real part, implying oscillations even though the system is overdamped (see **Figure 7a**). Just as in the case of a damped harmonic oscillator, the transition between exponential relaxation and damped oscillations is marked by an exceptional point (see **Figure 7a**), where the dynamical matrix D is not diagonalizable (194; see References 58 and 199 for an introduction to exceptional points). When the imaginary part of ω becomes positive, the solid can even become unstable (**Figure 7a**). In **Figure 5b**, an odd elastic phonon is shown for K° , μ , B > 0. Notice that the displacement field is circularly polarized; i.e., it traces out ellipses. A single point in the displacement field is shown as a function of time for an overdamped passive solid ($A = K^{\circ} = 0$; **Figure 5i**) and an overdamped odd elastic solid (K° , μ , B > 0; **Figure 5j**).

3.3. Odd Elastic Moduli and Energy Conservation

In Section 3.1, we stated that odd elastic moduli require a source of energy. In this section, we make this statement more precise and provide a derivation. To do so, we compute the work done by elastic forces when a solid quasistatically undergoes a closed cycle of deformations. If the work is nonzero along any closed loop, then the stress–strain relationship is not compatible with a potential energy.

3.3.1. Lagrangian and Eulerian coordinates. Before going to the main derivation, we make a brief technical aside. To make precise statements about stress, strain, and energy, it is useful to introduce the distinction between Eulerian coordinates and Lagrangian coordinates (200, 201). More detail is provided in the **Supplemental Text**, but the key idea is the following. When a material is deformed, a point originally at position x is moved to a new location X(x). Fields expressed in terms of x are said to be in Lagrangian coordinates, whereas fields expressed in terms of points in the lab (i.e., X), without reference to an undeformed state, are said to be in Eulerian

Supplemental Material >

¹³In the same way as in fluids (see Section 2.1.1), the six elastic moduli compatible with rotation symmetry are redundant from the point of view of the bulk elastodynamics equation: There are only four independent coefficients. Again, this ambiguity can be resolved if the stress tensor can be directly measured or imposed.

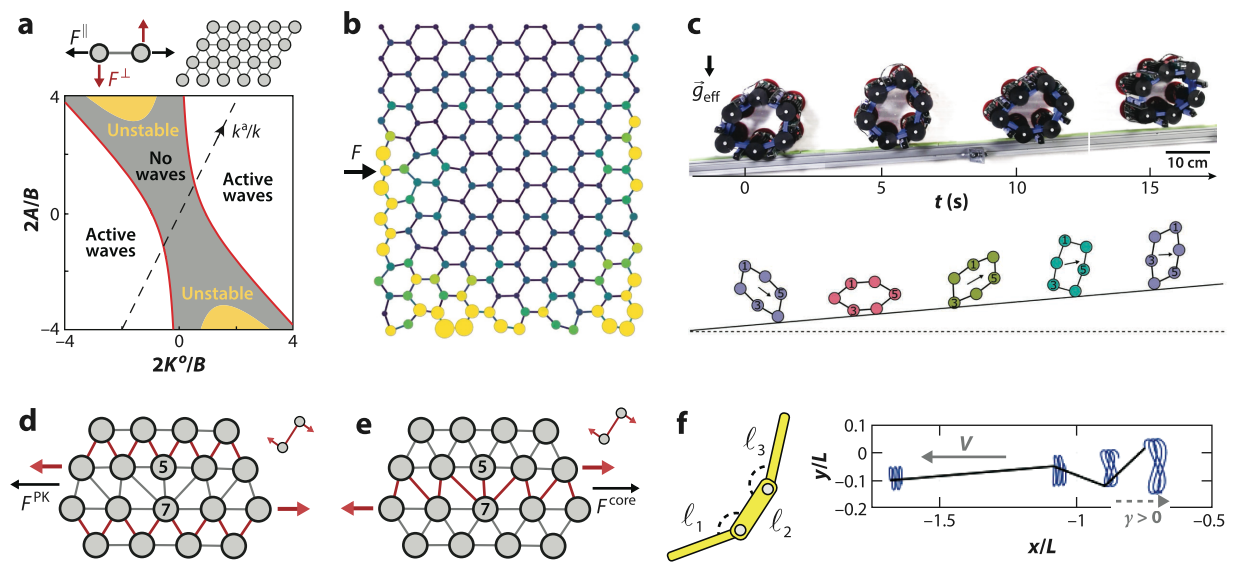


Figure 7

Phenomenology of odd elastic systems. (a) Phase diagram of an overdamped odd elastic solid in the continuum. Regions with no wave propagation (gray) are separated from regions of active wave propagation (white) by red boundaries marked by exceptional points of the dynamical matrix. In addition, the solid can become linearly unstable (yellow regions). The dashed line corresponds to a triangular lattice formed from masses and springs with transverse interactions (upper panel; see Equations 42 and 43); the corresponding elastic moduli are given by Equations 45 and 46. Adapted with permission from Reference 194. Copyright 2020 Springer Nature. (b) A honeycomb lattice is formed from masses and springs with transverse interactions (see Equation 42). When the system is poked at the side (black arrow), a unidirectional wave propagates at the boundary. Color and size are proxies for displacement. This wave is protected by a topological invariant known as the Chern number. Panel adapted with permission from Reference 195; copyright 2020 American Physical Society. (c) The active hinge from Figure 6i is configured in a hexagon. Such a hexagon undergoes an instability that propels it up a ramp. Panel adapted from Reference 220. (d) A triangular lattice of bonds experiencing a clockwise transverse force forms an odd elastic solid. A topological defect called a dislocation is embedded in the lattice: It consists of a particle with only five neighbors (labeled 5) paired with a particle with seven neighbors (labeled 7; other particles have six neighbors). The horizontal line separating these two particles is called the glide plane. The transverse forces from the bonds not crossing the glide plane (highlighted in red) give rise to opposing lateral forces on the rows of atoms containing the 5 and the 7. These forces motivate the dislocation to travel left and can be captured by a continuum notion known as the Peach-Koehler force F^{PK} . (e) The bonds that straddle the glide plane push in the opposite direction and, therefore, motivate the dislocation to move to the right. This effect has been referred to as a core force, Fore (197), which evades a continuum description. The core force vanishes when the microscopic interactions are entirely longitudinal. (f) A linkage system using the active hinge from Figure 6i, now with different length rods, undergoes shape changes that power swimming at low Reynolds number. Time traces of the joints are shown, and V represents the average velocity. Panel adapted from Reference 315.

coordinates.¹⁴ Depending on whether Lagrangian or Eulerian coordinates are used, there are two distinct versions of the stress tensor, respectively called the Piola–Kirchhoff (Lagrangian) stress P_{ij} and the Cauchy (Eulerian) stress σ_{ij} . In practice, one can often ignore the distinction between σ_{ij} and P_{ij} in linear elasticity, especially when there is no stress prior to deformation.¹⁵

¹⁴The fluid mechanics described in Section 2 is formulated entirely in terms of Eulerian coordinates. By contrast, derivations in elasticity are often easier in Lagrangian coordinates because the undeformed state is physically meaningful.

¹⁵To see why the distinction between the Piola–Kirchhoff and Cauchy stresses can often be ignored, it is useful to convert them into each other. They are related by $P_{ik}J_{jk}=(\det J)\,\sigma_{ij}$, where $J_{ij}=\frac{\partial X_i}{\partial x_j}=\delta_{ij}+\partial_j u_i$ is the Jacobian of the map X, and u(x)=X(x)-x is the displacement field. When there is no prestress,

3.3.2. Betti's theorem and Maxwell–Betti reciprocity. To set up the main derivation, we recall that the elasticity tensor in linear elasticity is the proportionality coefficient between the stress and the displacement gradient. The goal is to relate tensorial symmetries of the elasticity tensor to energy conservation. Our derivation is easiest in Lagrangian coordinates, in which linear elasticity takes the form

$$P_{ij} = P_{ij}^{\text{(pre)}} + C_{ijk\ell}^{\text{PK}} \, \partial_{\ell} u_k. \tag{34}$$

In Equation 34, $P^{\text{(pre)}}$ is the prestress present prior to deformations, u(x) = X(x) - x is the displacement field, $\partial_i u_j$ are displacement gradients, and $C_{ijk\ell}^{PK}$ is the elasticity tensor relating the Piola-Kirchhoff stress to displacement gradients. The forces due to the elastic stresses are given by $f_i = \partial_i P_{ij}$. When a material is deformed, the power exerted by the elastic forces is given by

$$\dot{W} = \int f_i \dot{u}_i d^d x = \int (\partial_j P_{ij}) \dot{u}_i d^d x = \int (\partial_j P_{ij}^{(\text{pre})} + C_{ijk\ell}^{\text{PK}} \partial_j \partial_\ell u_k) \dot{u}_i d^d x.$$
 35.

Upon performing an integration by part, we find that the elastic part of the power is

$$\dot{W}^{\text{el}} = -\int C_{ijk\ell}^{\text{PK}}(\partial_j \dot{u}_i)(\partial_\ell u_k) d^d x, \qquad 36.$$

in which we have ignored boundary terms and assumed that the elastic tensor $C_{ijk\ell}^{PK}$ is uniform.

The goal now is to compute the total elastic work done during a cyclic evolution in time in which the material is deformed and then returned to its initial state. By integrating Equation 36 over time, we find that the work is

$$\Delta W^{\text{el}} = \int \dot{W}^{\text{el}} dt = \int dt \, d^d x \, C^{\text{PK}}_{ijk\ell}(\partial_j \dot{u}_i)(\partial_\ell u_k) = -\int dt \, d^d x \, C^{\text{PK}}_{ijk\ell}(\partial_j u_i)(\partial_\ell \dot{u}_k), \tag{37}$$

in which the last equality is obtained from an integration by parts in time. After relabeling indices and summing the two equalities in Equation 37 we end up with

$$\Delta W^{\text{el}} = \int \dot{W}^{\text{el}} dt = -\int dt \, d^d x \, C_{ijk\ell}^{\text{PK,A}}(\partial_j \dot{u}_i)(\partial_\ell u_k).$$
 38.

Only the antisymmetric part $C_{ijk\ell}^{PK,A} = (C_{ijk\ell}^{PK} - C_{k\ell ij}^{PK})/2$ of the elasticity tensor appears in Equation 38. This leads to the central result: If $C_{ijk\ell}^{\text{PK,A}} \neq 0$, then there is always some cyclic deformation such that $\Delta W^{el} \neq 0$. This result is known as Betti's theorem (194, 202), and there are many equivalent statements. For example, the total work done by an elastic medium under an arbitrary deformation depends only on the final and initial states if and only if $C_{ijk\ell}^{PK,A} = 0$. Equivalently, $C_{ijk\ell}^{\mathrm{PK,A}} = 0$ if and only if there is a potential V such that $P_{ij} = \partial V/\partial(\partial_j u_i)$. The symmetry of the elasticity tensor $C_{ijk\ell}^{PK}$ is known as Maxwell–Betti reciprocity (202, 203).

3.3.3. Conversion between Cauchy and Piola-Kirchhoff stresses. In the above derivation (Section 3.3.2), we have used the Piola-Kirchhoff stress and Lagrangian coordinates.¹⁶ However, it is sometimes useful to work with the Cauchy stress σ_{ii} because it does not make reference to the undeformed material, and it is symmetric when angular momentum is conserved (see the sidebar titled Antisymmetric Stress). Just as with the Piola-Kirchhoff stress, we may expand the Cauchy stress as

$$\sigma_{ij} = \sigma_{ij}^{(\text{pre})} + C_{ijk\ell} \partial_{\ell} u_k,$$
39.

Supplemental Material >

Maxwell-Betti

displacements

reciprocity: symmetry

of the linear response matrix $C_{ijk\ell}^{PK}$ relating

www.annualreviews.org • Odd Viscosity and Elasticity

 $P_{ij} = \sigma_{ij} + \mathcal{O}(\partial_i u_j)^2$ at first order in displacement gradients. In all of Section 3, $\partial_i = \partial/\partial x_i$, where x_i is a position in the undeformed reference state. In Section 2, $\partial_i = \partial/\partial X_i$, where X_i is a fixed (Eulerian) position in the lab. See the **Supplemental Text** for further discussion.

¹⁶Lagrangian coordinates are required to permute the time and space derivatives between Equations 36 and 37.

where $\sigma_{ij}^{\text{(pre)}}$ is the (Cauchy) prestress present even in the undeformed medium. We emphasize that $C_{ijk\ell}$ is different from $C_{ijk\ell}^{PK}$ because it relates the Cauchy stress, not the Piola–Kirchhoff stress, to the displacement gradients. As shown in the **Supplemental Text**, the two tensors are related to linear order in strain by (197)

$$C_{ijk\ell}^{\text{PK}} = C_{ijk\ell} + \sigma_{ij}^{\text{(pre)}} \delta_{k\ell} - \sigma_{i\ell}^{\text{(pre)}} \delta_{jk}.$$

$$40.$$

The takeaway from Equation 40 is that there is no distinction between $C_{ijk\ell}$ and $C_{ijk\ell}^{PK}$ when the prestress vanishes $\sigma_{ij}^{(pre)} = 0$. For the matrix in Equation 28 describing a 2D isotropic system, the conversion formula in Equation 40 yields

$$C_{\alpha\beta}^{\text{PK}} = \begin{bmatrix} B - \frac{p^{(\text{pre})}}{2} & \Lambda + \frac{\tau^{(\text{pre})}}{2} & 0 & 0\\ A - \frac{\tau^{(\text{pre})}}{2} & \Gamma - \frac{p^{(\text{pre})}}{2} & 0 & 0\\ 0 & 0 & \mu + \frac{p^{(\text{pre})}}{2} & K^{\text{o}} - \frac{\tau^{(\text{pre})}}{2}\\ 0 & 0 & -K^{\text{o}} + \frac{\tau^{(\text{pre})}}{2} & \mu + \frac{p^{(\text{pre})}}{2} \end{bmatrix}.$$
 41.

Hence, the constitutive relation in Equation 28 is compatible with a potential energy if and only if $A - \Lambda = 2\tau^{\text{(pre)}} = 2K^{\text{o}}$.

Equation 26 in Section 3.1 is valid only when the prestress vanishes (and to lowest order in gradients). When the prestress $\sigma_{ij}^{(\text{pre})}$ is nonzero, the correct expression is Equation 38, which features $C_{ijk\ell}^{PK}$ instead of $C_{ijk\ell}$. The expression in Equation 38 is correct to all orders in displacement gradients if the constitutive relation in Equation 34 is assumed to be exact.

3.3.4. Other geometries and constitutive relations. The above derivation applies to linear elasticity, in which the stress is linearly proportional to the strain. Going beyond linear elasticity, a stress–strain relationship $\sigma = f(\nabla u)$ is called hyperelastic if it is derived from a strain energy density (201). Another class of nonlinear constitutive relations specify the rate of change of the stress as a function of the velocity gradient by $\dot{\sigma} = f(\sigma, \nabla v)$, in which ∇v is the Eulerian velocity gradient tensor. Such constitutive relations are called hypoelastic (1) and can also be classified based on whether they require energy sources and/or dissipation. The above discussion was also framed in terms of Cauchy elasticity, in which the solid has the same dimension as the space it lives in. More generally, energy arguments can be considered for slender geometries (see Section 3.4.5); for constitutive relations involving memory or viscoelasticity (see Section 3.5.4); for elastoplasticity (204–209), hypoelasticity (210), and damage (211–213); and for materials with additional geometric degrees of freedom (214), such as the polymer alignment fields (215, 216) or micropolar degrees of freedom (217–219).

3.4. Where to Find Odd Elasticity?

We now turn to the following questions: What experimental systems display odd elasticity, and what are the key ingredients to observe it? Many systems exhibit the qualitative ingredients required for odd elasticity, and it has been suggested as an explanation for observed mechanical behavior in colloidal and biological systems (149, 157, 196). Odd elastic moduli have also been determined in realistic simulations of engineered metamaterials (219, 220).

3.4.1. Point particles with noncentral, pairwise interactions. The simplest microscopic picture of an elastic solid is a collection of masses connected by springs, or more generally, point particles interacting via pairwise forces (149, 194, 195, 197). This class of models can be described as follows. Let us consider N particles with positions $\mathbf{x}^{\alpha}(t)$, where α labels particles, and assume that the total interaction force $\mathbf{F}^{\alpha}(\mathbf{x}^{1}, \dots, \mathbf{x}^{N})$ only depends on the particle positions. This force is

VIOLATIONS OF NEWTON'S THIRD LAW

In most of this review, we have assumed that linear momentum is conserved. Microscopically, this means that when two constituents interact, they exert equal and opposite forces on each other (this is Newton's third law). At the continuum level, it means that interparticle interactions enter the balance of linear momentum equation as the divergence of a momentum current ($\nabla \cdot \sigma$). However, there are many systems in which linear momentum is effectively not conserved (at the level of description that is most convenient; when all degrees of freedom are kept in the description, the linear momentum of a closed system is conserved). These include collections of self-propelled particles such as birds or active colloids (221–225), particles interacting through hydrodynamic interactions (226–230) or through chemical fields (231–233), complex plasma (234), and optical matter (235–237). For solids, a gradient expansion of the continuum force density then takes the general form $f_i = f_i^0 + A_{ik}u_k + B_{ijk}\partial_ju_k + C_{ijk\ell}\partial_j\partial_\ell u_k$, where the familiar second derivative term due to elasticity is no longer the leading contribution (238). For example, in the context of microfluidic 1D crystals, one can derive a linear wave equation of the form (227)

$$\partial_t u = \alpha \partial_x u + \beta \partial_x^2 u.$$

The first term in this equation results from an effective violation of Newton's third law and is lower-order in gradients than one would expect from elasticity. It describes the advection of deformations. The full equation is an advection-diffusion equation. The dispersion $\omega(q) = \alpha q \neq \omega(-q)$ of waves described by this equation is asymmetric, in contrast with normal elastic waves (described by $\partial_t^2 u = \beta \partial_x^2 u$) for which $\omega(q) = \sqrt{\beta} |q| = \omega(-q)$. In 2D crystals, violations of Newton's third law have been shown to spontaneously drive dislocation motion (238). In addition, an effective interaction violating Newton's third law emerges between dislocations themselves in odd elastic crystals, even though the microscopic constituents obey Newton's third law (197).

said to be potential if $F_i^{\alpha} = -\partial V/\partial x_i^{\alpha}$ for some potential function $V(\mathbf{x}^1,\dots,\mathbf{x}^N)$. Here, we do not assume, as is often done, that the forces are potential. However, we focus on forces that respect Newton's third law, as these can be captured by a stress tensor in the continuum (see the sidebar titled Violations of Newton's Third Law for when this is not the case). Formally, Newton's third law means that the forces F^{α} can be decomposed as $F^{\alpha}(\mathbf{x}^1,\dots,\mathbf{x}^N) = \sum_{\beta} F^{\alpha\beta}(\mathbf{x}^1,\dots,\mathbf{x}^N)$ with $F^{\alpha\beta} = -F^{\beta\alpha}$.

For concreteness, let us focus on 2D systems with pairwise forces that are covariant under rotation. In this case, the force law takes the form $F^{\alpha\beta}(x^1, \dots, x^N) = F(x^{\alpha} - x^{\beta})$, where

$$F(r) = F^{\parallel}(r)\hat{r} - F^{\perp}(r)\hat{\phi}$$
42.

in which $\hat{r} = r/r$, r = ||r||, and $\hat{\phi} = -\epsilon \cdot \hat{r}$. As illustrated in **Figure 6a**, $F^{\parallel}(r)$ is a radial force, and $F^{\perp}(r)$ is a transverse force. The force law is noncentral when $F^{\perp} \neq 0$. Notice that such an interaction is compatible with a potential if and only if $\nabla \times F = \frac{1}{r} \partial_r (rF^{\perp}) = 0$. Except for the special case of $F^{\perp} \propto 1/r$ (relevant to vortices; see Section 3.4.2), the force is nonpotential if $F^{\perp} \neq 0$. As illustrated in **Figure 6b-g** and discussed in Sections 3.4.2 and 3.4.3, the model in Equation 42 has been used to describe systems ranging from biological and colloidal crystals to skyrmions and gyroscopic matter within the approximation of pairwise interactions.

Particles interacting via Equation 42 tend to form triangular lattices (also called hexagonal lattices). Linearizing about a perfect lattice with spacing *a*, we may write Equation 42 as

$$F^{\parallel}(r) \approx F^{\parallel}(a) - k(r - a) \qquad \qquad F^{\perp}(r) \approx F^{\perp}(a) - k^{a}(r - a). \tag{43}$$

The linearized interactions in Equation 43 can be thought of as (odd) Hookean springs with spring constant k and a transverse spring constant k^a . When F(r) falls off sufficiently rapidly, a useful

approximation is to keep only the interactions between nearest neighbors. In this approximation, the ambient pressure $p^{\text{(pre)}}$ and ambient torque $\tau^{\text{(pre)}}$ in a triangular lattice are

$$p^{\text{(pre)}} = \sqrt{3} \frac{F^{\parallel}(a)}{a}$$
 $\tau^{\text{(pre)}} = -\sqrt{3} \frac{F^{\perp}(a)}{a},$ 44.

and the isotropic 2D elastic moduli are

$$B = \frac{\sqrt{3}}{2} \left(k + \frac{F^{\parallel}(a)}{a} \right) \qquad \qquad \mu = \frac{\sqrt{3}}{4} \left(k - \frac{3F^{\parallel}(a)}{a} \right)$$
 45.

$$A = -\frac{\sqrt{3}}{2} \left(k^a + \frac{F^{\perp}(a)}{a} \right) \qquad K^{o} = \frac{\sqrt{3}}{4} \left(k^a - \frac{3F^{\perp}(a)}{a} \right). \tag{46}$$

We see explicitly from Equation 46 that the transverse force gives rise to odd elastic moduli. We refer to References 8, 16, 17, 194, 197, 238, and 242–245 for more details on the coarse-graining procedures and to Reference 246 for situations in which disorder is included.

3.4.2. Skyrmions, vortices, and gyroscopes. Describing the motion of particles in lossy environments (such as colloids in water) and quasiparticles such as topological defects often involves a mobility matrix μ , such that $\dot{x} = \mu \cdot \tilde{F} \equiv F$, where $\tilde{F} = -\nabla V$ is potential. Such an equation of motion arises, for example, in collections of fast-spinning, pinned gyroscopes connected by springs (239, 247–255), skyrmions (256–261), and vortices in superfluids¹⁷ (262–270); see **Figure** 6*d*,*e*. These systems typically form triangular lattices; odd elasticity can also occur in less ordered systems, provided that they are rigid.

By coarse graining the forces F (e.g., via the Irving–Kirkwood formula; 17), we obtain a continuum equation of motion of the form $\gamma \partial_t u_i = \partial_j \sigma_{ij}$, where $\sigma_{ij} = C_{ijk\ell} \partial_\ell u_k$ and γ is a scalar drag coefficient. If μ is asymmetric, then $C_{ijk\ell}$ contains odd elastic moduli. Furthermore, if μ is isotropic in two dimensions, then it is proportional to a rotation matrix $R(\theta)$. The effect of μ is then to rotate by an angle θ all the interparticle forces that there would be in a standard overdamped solid. In this case, the nonzero odd elastic moduli are A and K^o , and they are constrained to the ratio $A/B = K^o/\mu = \tan \theta$.

An equivalent coarse-graining method starts with the equation of motion $[\mu^{-1}] \cdot \dot{x} = \tilde{F}$, where now the mobility matrix is written on the left-hand side. Written this way, one is led to coarse grain the force \tilde{F} instead of F. This is a common approach for systems governed by a Lagrangian of the form $L = \sum_{\alpha} x^{\alpha} \cdot \epsilon \cdot \dot{x}^{\alpha} - V(x^{1}, \dots, x^{N})$ such as skyrmions or gyroscopes (264, 265). We then obtain a continuum equation of motion of the form $\gamma_{ik}\partial_{t}u_{k} = \partial_{j}\tilde{\sigma}_{ij}$, where $\tilde{\sigma}_{ij} = \tilde{C}_{ijk\ell}\partial_{\ell}u_{k}$ and $\gamma = \gamma \mu^{-1}$. Because \tilde{F} is conservative, the elasticity tensor $\tilde{C}_{ijk\ell}$ has no odd elasticity. However, the complexity has been transferred into the structure of the effective drag coefficient γ which is now a tensor. Not all combinations of odd elastic moduli can be obtained in this way. Whenever $A/B \neq K^{\circ}/\mu$, the elastic moduli are not compatible with an asymmetric mobility matrix (195, 197). Likewise, odd elasticity does not capture all of gyroscope mechanics: When not in the fast spinning limit, gyroscopic systems give rise to a distinct theory known as gyroelasticity (see the sidebar titled Gyroelasticity).

 $^{^{17}}$ Skyrmions and superfluid vortices are topological objects in the magnetic and velocity field, respectively. They both experience a so-called Magnus force that gives rise to their transverse interactions. Superfluid vortices have an interaction that goes as 1/r for sufficiently large separation, resulting in complex dynamics that evade standard elasticity (262).

GYROELASTICITY

Gyroelasticity provides a continuum description for networks of coupled gyroscopes (239, 247–256). Consider tracking the displacement x of the tip of a gyroscope pinned to the ceiling. For small deflections, the tip responds to a Newtonian force \tilde{F} as

$$(m\delta_{ij}\partial_t^2 + \alpha\epsilon_{ij}\partial_t)x_j = \tilde{F}_i,$$

where α is proportional to the angular momentum of the gyroscope (248). In the continuum, the force density in a network of gyroscopes is the divergence of the stress $\tilde{F}_i = \partial_j \tilde{\sigma}_{ij}$, where $\tilde{\sigma}_{ij} = \tilde{C}_{ijk\ell} \partial_\ell u_k$. In the limit that $\alpha \to 0$, one obtains standard elasticity. In the limit that $m \to 0$, we can rewrite the equations as $\alpha \partial_r x_i = \epsilon_{ij} \tilde{F}_j$. Because the motion is perpendicular to the force, as discussed in Section 3.4.2, it is useful to define an effective stress $\sigma_{ij} = \epsilon_{ik} \tilde{\sigma}_{kj}$. Defined this way, the effective stress–strain relationship $\sigma_{ij} = C_{ijk\ell} \partial_\ell u_k$ has odd elasticity (though the stress does not correspond to linear momentum transfer). In general, gyroelasticity interpolates between odd elasticity with first-order dynamics and standard elasticity with second-order dynamics. Topological boundary modes and other chiral waves have been studied extensively in these systems (239, 247–256).

The systems discussed in this section share an important conceptual feature: The stress tensor σ_{ij} does not represent the flux of linear momentum, and the work $\delta W = F \cdot \delta x$ does not represent a physical energy. For example, quasiparticles such as vortices or skyrmions do not have mass or linear momentum in the usual sense. Likewise, the motion of the tips of pinned gyroscopes is governed by the transfer of angular momentum (not linear momentum) because the gyroscopes are anchored to a substrate. In the same way, submerged particles at low Reynolds number discussed in Section 3.4.3 are not ruled by linear momentum conservation, as they continually exchange momentum with the fluid. In these situations, the equations of motion are a firmer starting point than the mechanical notions of force or work.

3.4.3. Spinning particles at low Reynolds number: from driven colloids to starfish embryos.

The interactions in Equation 42 have been used to model 2D aggregates of particles driven to spin at low Reynolds number. As shown in **Figure 6b**,c,f,g, examples include Janus particles (148), magnetic colloids (149), spinning bacteria (271), swimming algae (272), and starfish embryos, for which the values $A/\mu \approx 8$ and $K^{\rm o}/\mu \approx 7$ have been reported (157). The fluid mechanics in these systems involves a complex interplay among electromagnetic interactions, steric contact between particles or with the substrate, and particle shape change (such as ciliary and flagellar motion). Odd elasticity has been suggested (149, 157) as a natural ingredient in the continuum theory because the fluid-mediated force between two spinning particles has a nonzero transverse component (273–275), thus resembling the model in Equation 42. Open challenges include the systematic coarse graining of the particle system with nonpairwise and long-range hydrodynamic interactions into an effective continuum theory and the role of additional order parameters (such as the angular velocity of the particles) in this description.

3.4.4. Active hinges: odd elasticity with conserved angular momentum. In an inertial system, the transverse force in Equation 42 inherently requires a torque to be provided to each bond. The building blocks must therefore have an internal or external reservoir of angular momentum. However, such a reservoir is not necessary for odd elasticity in systems with nonpairwise interactions (194). For example, the linkage shown in **Figure** 6i has two angular degrees of freedom, θ_1 and θ_2 , each determined by the location of three vertices. When an angle deforms, it experiences

a torsional force τ_i proportional to the change in angle $\delta\theta_i$, for example, given by

$$\begin{bmatrix} \tau_1 \\ \tau_2 \end{bmatrix} = \begin{bmatrix} -\kappa & \kappa^a \\ -\kappa^a & -\kappa \end{bmatrix} \begin{bmatrix} \delta\theta_1 \\ \delta\theta_2 \end{bmatrix}.$$
 47.

Here, κ is the standard bond bending stiffness provided, for example, by the elastic band subtending the joint. The coefficient κ^a is an antisymmetric coupling that would not appear in passive systems. Both the usual bond bending stiffness and the odd bending stiffness describe nonpairwise interactions because the angle at each vertex (and hence the force) is determined by the locations of three vertices. The active hinge described by Equation 47 can be realized, for example, in robotic metamaterials with internal motors (see **Figure 6i** and Reference 220). For this system, the power done by the torsional forces is $\dot{W} = \tau_i \dot{\theta}_i$, so the work done along a closed cycle vanishes if and only if $\kappa^a = 0$. Hence, the torque–angle relationship is nonconservative when $\kappa^a \neq 0$. Consequently, a lattice made of such units (**Figure 6i**) generically exhibits odd elasticity in the continuum limit. Because the microscopic building block has no unbalanced torques, A = 0 and $\tau^{(\text{pre})} = 0$ in the continuum description.

3.4.5. Slender geometries: from robotic beams to muscles and biomembranes. So far, we have primarily considered 2D isotropic media confined to the plane, but this need not be the case. For example, Figure 6j shows a quasi-1D metamaterial in which each unit cell consists of three piezoelectric patches mounted on a steel beam (219). The beam has two modes of deformation, bending (Figure 6j, left) and shearing (Figure 6j, right). These modes of deformation in turn induce a shear stress σ and a bending moment, M. The constitutive relation between the two takes the form

$$\begin{bmatrix} \sigma \\ M \end{bmatrix} = \underbrace{\begin{bmatrix} \mu & P \\ 0 & B \end{bmatrix}}_{C} \begin{bmatrix} s \\ b \end{bmatrix}.$$
 48.

The matrix C plays the role of the elasticity tensor, and μ and B are the shear and bending moduli, respectively, that one would expect from Timoshenko–Ehrenfest beam theory (276). An electronic feedback between the piezoelectric patches induces an additional modulus P. Because the energy differential is $\delta W = \sigma \delta s + M \delta b$, the asymmetric part of C corresponds to a violation of Maxwell–Betti reciprocity and therefore requires a source of energy. The parity-violating and nonconservative modulus P also induces unidirectional wave amplification (219).

Theoretical designs for 2D piezoelectric odd elastic materials have been proposed (277). In addition to quasi-1D structures (219, 220), three-dimensional solids (194, 196), thin membranes (278), and moderately thick plates (279) have been considered. Odd elasticity can also emerge, in principle, from more complex building blocks. For example, as illustrated in **Figure** 6*k*, it has been recently suggested that muscle tissue in suitable operating regimes can be approximately modeled as a 3D anisotropic odd elastic medium (196, 280).

3.4.6. Phase diffusion in pattern formation: rotating Rayleigh–Bénard convection. Although elasticity is often associated with solid media, it can also refer more broadly to the tendency of a pattern to resist deformation. For instance, in Rayleigh–Bénard convection a fluid is confined between two horizontal plates at different temperatures, with the hot plate below. When the temperature difference is large enough, an instability develops, leading to the appearance of spatial patterns (281–283). For example, **Figure 6***b* shows a triangular lattice of hexagonal convection

NONVARIATIONAL DYNAMICS OF ORDER PARAMETERS

In systems with spontaneously broken symmetries such as critical phenomena and pattern formation, the dynamics of the order parameter X can be modeled by a dynamical system $\partial_t X = f(X)$. Such a dynamical system is called nonvariational (or nonpotential) when it is not possible to locally express f as the gradient of a potential ($f_i \neq -\partial_i V$; 288–294). In this case, the Jacobian $J_{ij} = \partial_i f_j \neq J_{ji}$ is not symmetric. In contrast, for potential systems, it must be symmetric as $J_{ij} = -\partial_i \partial_j V = J_{ji}$. This is reminiscent of odd elasticity and odd viscosity, but here the antisymmetry enters at the level of the linearized equations of motion rather than in the constitutive relations. The nonvariational nature of the dynamics leads to various effects that would not occur in purely relaxational systems, including time-dependent states with complex spatiotemporal structure, some of which have been experimentally observed (295, 296). These include rotating spiral states (295); self-propelled localized structures such as dislocations, Bloch walls, and defects moving at constant speed (283, 291, 292, 294, 296–300); proliferation of defects (298, 299); localized pulses (295); spontaneous parity breaking and traveling states (288, 293, 301–303); and spatiotemporal chaos (288, 295, 304, 305). When a noise term is added to the dynamical system, the nonvariational nature of the dynamics is typically associated with broken time-reversal invariance, a nonvanishing rate of entropy production in the steady state (289, 290, 306), and nonreciprocal couplings or interactions (307, 308).

cells. Pattern formation is an instance of spontaneous symmetry breaking, in the same way that translational symmetry is broken by a solid. Large wavelength modulations of the pattern are therefore slow variables that describe the elastic response of the pattern: Gentle perturbations tend to relax in the same way as disturbances in an overdamped crystal.

In rotating Rayleigh–Bénard convection, the fluid is put under rotation (284–287), leading to Coriolis forces and a nonvariational dynamics for the order parameter describing the pattern (see the sidebar titled Nonvariational Dynamics of Order Parameters). The relaxation of the pattern is then described by an equation of motion formally identical to that of elastodynamics. To see that, let us describe a slightly deformed hexagonal pattern as

$$T(\mathbf{x},t) = T_0 \sum_{j} e^{i\mathbf{q}_{j} \cdot [\mathbf{x} - \mathbf{u}(t,\mathbf{x})]} + \text{c.c.},$$

$$49.$$

in which T is the temperature field in a horizontal plane (other variables can be deduced from T); $\mathbf{q}_1 = (0,1)$, $\mathbf{q}_2 = (-\sqrt{3}/2, -1/2)$, and $\mathbf{q}_3 = (\sqrt{3}/2, -1/2)$ are the wave vectors of the Fourier modes producing the hexagonal pattern; $\mathbf{u}(\mathbf{x},t)$ is a slow phase shift describing the deformation of the pattern; T_0 a constant; and c.c. means complex conjugate. The dynamics of the effective displacement field $\mathbf{u}(\mathbf{x},t)$ is then (309–311)

$$\partial_t \mathbf{u} = D_{\parallel} \nabla (\nabla \cdot \mathbf{u}) + D_{\perp} \Delta \mathbf{u} + D_{\parallel}^{\times} \boldsymbol{\epsilon} \cdot \nabla (\nabla \cdot \mathbf{u}) + D_{\perp}^{\times} \boldsymbol{\epsilon} \cdot \Delta \mathbf{u},$$
 50.

where $D_{\parallel}, D_{\perp}, D_{\parallel}^{\times}$, and D_{\perp}^{\times} are termed phase diffusivities. Equation 50 is identical to the equation of motion (Equation 31) of an overdamped ($\rho \to 0$) 2D isotropic odd elastic system, with the phase diffusivities playing the role of the elastic moduli: $D_{\parallel} = B/\gamma$, $D_{\perp} = \mu/\gamma$, $D_{\parallel}^{\times} = -A/\gamma$, and $D_{\perp}^{\times} = K^{\circ}/\gamma$. We emphasize that although the displacement field is a slow variable in these systems, there is a priori no distinguished notion of stress or particle in the system.

3.5. Odd Elastic Phenomenology

The presence of odd elastic moduli and microscopic nonconservative forces gives rise to distinctive phenomena. Below we detail these effects, which range from self-propelled topological defects to topological waves.

3.5.1. Topological defects. A crystalline topological defect is an imperfection in a crystal structure that cannot be removed by local rearrangements of the particles (see References 102, 198, and 312–314 for an introduction). These defects act as quasiparticles, and their motion governs the large-scale rearrangement of the crystal. For example, in a hexagonal lattice, an extra row of atoms inserted into the crystal structure typically results in a pair of atoms with five and seven neighbors (in a Voronoi tessellation) known as a dislocation (see **Figure 7d**). The dislocation carries a topological charge, the Burgers vector $b_j = \oint \partial_i u_j dr_i$, where the contour encloses the dislocation of interest. Transverse forces as in Equation 42 fundamentally modify how the defects move and interact. Spontaneous dislocation motion and nucleation have been reported in experiments on colloidal crystals (148, 149). In addition, theoretical arguments suggest that the interaction between defects can become nonmutual (197). Even without defect motion, transverse forces can also modify the static strain around stationary topological defects (157, 197).

For example, a dislocation is said to glide when the two rows of atoms containing the fivefoldand sevenfold-coordinated particles slide past each other. The dislocation moves in the same direction as the fivefold particle. For forces with a clockwise handedness, the bonds that do not cross the glide plane favor dislocation motion to the right, as shown in Figure 7d. However, the bonds that cross the glide plane push the dislocation in the opposite direction (as shown in Figure 7e). These two effects are in competition with each other. The effect of the bonds that do not cross the glide plane can be captured by a continuum notion known as the Peach-Koehler force, $F_i^{\text{PK}} = -b_k \sigma_{kj}^{(\text{pre})} \epsilon_{ji}$, where b_k is the Burgers vector (102, 312–314), and $\sigma_{ij}^{(\text{pre})} = \tau^{(\text{pre})} \epsilon_{ij}$ is the torque density induced by microscopic transverse forces (149, 197, 238). The contribution from the bonds that cross the glide plane evades a continuum explanation, because it arises from a difference in forces separated by one lattice spacing a. Nonetheless, this small length-scale effect can be captured by a microscopic core force $F^{\text{core}} = \frac{1}{a} \int_{\mathcal{C}} F(r) \cdot dr$, where F(r) is the microscopic interaction, and \mathcal{C} is an integration contour defined by microscopic particle trajectories (197). When the transverse forces are strong enough, the defects can spontaneously glide in a direction determined by the stronger of the two forces F^{PK} or F^{core} . More generally, the interactions between topological defects (mediated by elastic strains) do not fall within the typical paradigm of conservative field theories (see also the sidebar titled Nonvariational Dynamics of Order Parameters). An open question, relevant for systems ranging from skyrmion lattices (257) to complex fluids (148, 149), is how modified defects dynamics affect the nature of plastic deformation and melting.

- **3.5.2.** Topological waves. Nonconservative forces can be useful for constructing mechanical systems with nontrivial band topology (see References 58, 59, and 199 for introductions to topological waves). Networks of bonds obeying Equation 42 can behave as so-called Chern insulators (194, 195, 316), where unidirectional edge modes can propagate at the boundary of the system (see **Figure 7b**). Because the forces are nonconservative, the dynamical matrix governing the linear waves is in general non-Hermitian, leading to features such as the non-Hermitian skin effect, in which the bulk modes are localized at one edge of a 1D system, and exceptional points, in which the eigenvectors of the dynamical matrix do not span the Hilbert space (58, 199). For instance, unidirectionally amplified waves arising from the non-Hermitian skin effect have been observed in the beam in **Figure 6***i* (219) and in 1D chains of the active hinges in **Figure 6***i* (220). We refer to Reference 196, and references therein, for more details.
- **3.5.3.** Nonlinearities and noise. In solids with energy injection, instabilities are generic. For example, when $\rho \neq 0$ and K^{o} is sufficiently large, the linear odd elastic waves described by Equation 32 become unstable (194; see **Figure 7***a*). Either a linear instability results in the

destruction of solid material or it must be stabilized by nonlinearities, leading to nonlinear dynamical structures such as limit cycles and chaotic attractors. For example, consider a single particle attached to the origin by a force law of the form of Equation 42:

$$\gamma \begin{bmatrix} \dot{u}_x \\ \dot{u}_y \end{bmatrix} = - \begin{bmatrix} k & k^a \\ -k^a & k \end{bmatrix} \begin{bmatrix} u_x \\ u_y \end{bmatrix} - k' \|\boldsymbol{u}\|^2 \begin{bmatrix} u_x \\ u_y \end{bmatrix},$$
 51.

where $\mathbf{u} = (u_x, u_y)$ is the displacement of the particle from the origin, $\gamma > 0$ is a damping rate, k is the normal spring constant, k^a is the odd spring constant, and k' > 0 is a nonlinear spring constant. When k changes from positive to negative, the system bifurcates from having a stable fixed point to a stable limit cycle through a Hopf bifurcation (see, e.g., 317), after which the displacement rotates at a fixed frequency in the plane.

Limit cycles and other attractors can prove useful, for instance, to realize locomotion (318). For example, in Reference 220, when the active hinges from Section 3.4.4 are put on a ring, the force law and dissipation create a limit cycle of shear deformations. When the ring is placed on a ramp, the limit cycle causes repeated contact with the surface, allowing the ring to propel itself, even against gravity (see **Figure 7***c*). In References 315 and 319 the active hinge is immersed in a viscous fluid, and the limit cycle results in swimming behavior (see **Figure 7***f*). The interplay between nonconservative forces and noise has also been studied (320, 321). In the context of the swimming hinges, it is shown that random fluctuations give rise (on average) to persistent motion (315, 319).

3.5.4. Odd viscoelasticity. The linear response of a material need not be instantaneous in time. To take a finite-time response into account, the mechanical response of a material to deformations can be captured by the equation

$$\sigma_{ij}(t) = \int_{-\infty}^{\infty} M_{ijk\ell}(\tau) \partial_{\ell} \dot{u}_k(t-\tau) d\tau,$$
52.

in which a finite-time response kernel $M_{ijk\ell}(t)$ has been introduced, in a way similar to electrodynamics in materials (32, 322, 323). Viscosity and elasticity are special cases with $M_{ijk\ell}(\tau) = \eta_{ijk\ell}\delta(\tau)$ and $M_{ijk\ell}(\tau) = C_{ijk\ell}\Theta(\tau)$, where $\Theta(\tau)$ is a Heaviside step function. In the same way as for viscosity and elasticity, a medium is called odd viscoelastic when

$$M_{ijk\ell} \neq M_{k\ell ij}$$
. 53.

A coefficient in the antisymmetric part of $M_{ijk\ell}$ is termed an odd viscoelastic modulus. The work done over a closed cycle of deformation of period T is given by 18

$$\Delta W = \int_0^T \sigma_{ij} \partial_j \dot{u}_i(t) dt = -i \sum_{\omega} \omega \sigma_{ij}(\omega) \partial_j \bar{u}_i(\omega) = -\sum_{\omega} \omega^2 \partial_j \bar{u}_i(\omega) M_{ijk\ell}(\omega) \partial_\ell u_k(\omega), \quad 54.$$

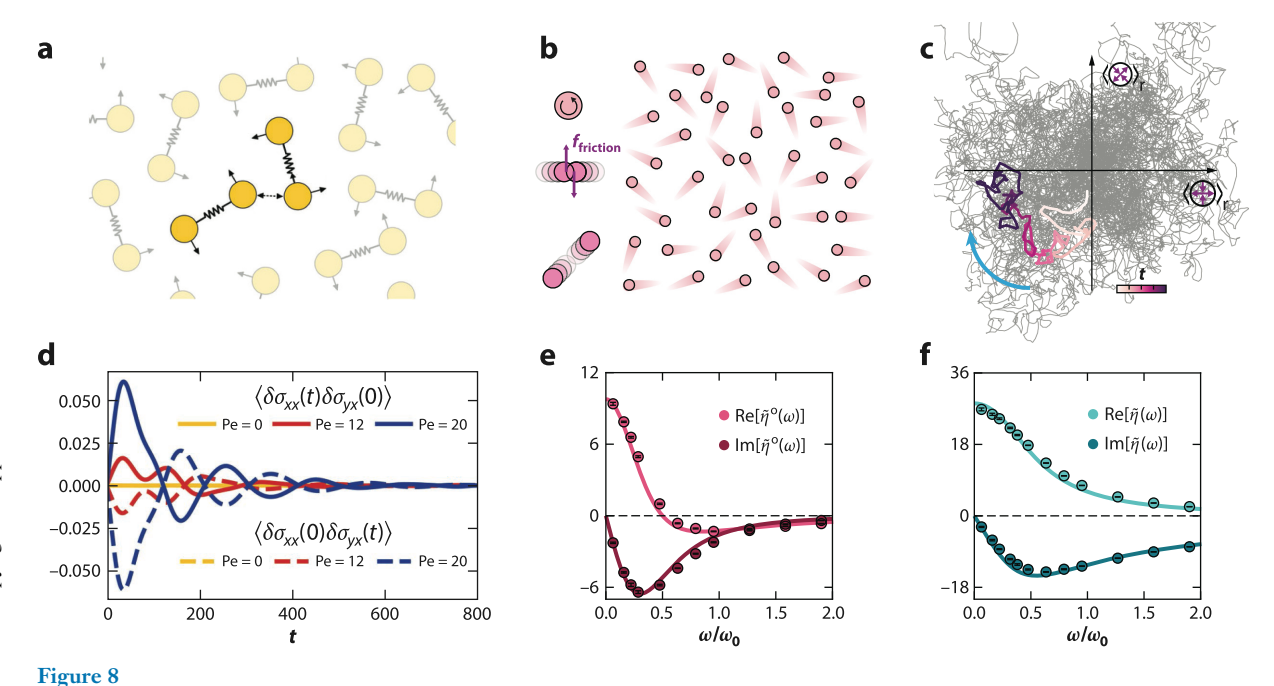
where the sum is over $\omega = 2\pi n/T$ for integer n, and the overline represents complex conjugation (149, 196, 219, 324). When the material is passive, the work must be nonpositive for all possible cycles, which implies that $M_{ijk\ell}(\omega)$ (viewed as a linear operator on rank two tensors, for instance, using the matrix representation of Sections 2.1.1 and 3.2.1) must be positive semidefinite for all frequencies ω (325–327). In rheology, $M_{iik\ell}(\omega)$ is often written as

$$i\omega M_{ijk\ell}(\omega) = G'_{ijk\ell}(\omega) + iG''_{ijk\ell}(\omega),$$
 55.

where the storage modulus $G'_{ijk\ell}$ contains (odd and even) elasticity, and the loss modulus $G''_{ijk\ell}$ contains (odd and even) viscosity. The adjectives "loss" and "storage" are misnomers when

Odd viscoelastic modulus: an antisymmetric component of the linear response tensor $M_{iik\ell}$

¹⁸For simplicity, we are ignoring the distinction between the Piola–Kirchhoff and the Cauchy stresses in this discussion.



Fluctuating hydrodynamics of odd viscoelastic fluids. (a) A collection of dumbbells subject to active torques interacting with each other and (b) a collection of spinning granular particles interacting with each other; each forms a chiral active fluid. (c) The evolution of the fluctuating space-averaged stress in the system of panel b can be described as a chiral random walk in the space of shear stresses, whose correlations contain normal and odd shear viscosities. (d) Stress–stress correlations in the system of panel a. The viscosities are related to the stress–stress correlations through a Green–Kubo formula (see Section 2.3.1). Here, the component η_{xxyx} is considered. (e, f) The Fourier-Laplace-transformed stress–stress correlations of the system of panel b can be seen as complex-valued frequency-dependent viscoelastic moduli $\tilde{\eta}(\omega)$ and $\tilde{\eta}^{o}(\omega)$. Here, ω_{0} is a characteristic frequency related to the tumbling time required for a particle to randomize its direction (6). Panels d-f show that the systems described in panels a and b exhibit an odd viscoelastic response. The

complex shear viscosity $\eta(\omega) = \eta'(\omega) - i\eta''(\omega)$ is related to the (complex) dynamic shear modulus $G(\omega) = G'(\omega) + iG''(f)$ through $\eta' = G''/\omega$ and $\eta'' = G'/\omega$, where ω is the angular frequency (322). Panels a and d adapted with permission from Reference 82. Panels b,

antisymmetric terms are present: The antisymmetric part of $G''_{ijk\ell}$ does not contribute to dissipation, and the antisymmetric part of $G'_{ijk\ell}$ is capable of injecting or dissipating energy. Importantly, at finite frequency, passive materials can still have an antisymmetric component of $G'_{ijk\ell}$ so long as $M_{ijk\ell}$ remains positive-definite.

Odd viscoelasticity has been considered in the context of minimal spring-dashpot models (328), instabilities in chiral crystals (149), and quantum Hall effects with a tilted magnetic field (85), and in simplified models of muscles (196, 280). The competition between viscosity and elasticity has been suggested as a mechanism for wavelength selection at the onset of instability (149, 194). Notably, the frequency dependence of $G'_{ijk\ell}$ and $G''_{ijk\ell}$ has been measured in numerical simulations of chiral active fluids (see **Figure 8** and References 6 and 82), where it can be captured by simple analytical models (6).

4. CONCLUSION

c, e, and f are adapted with permission from Reference 6, copyright 2021 Springer Nature.

In this review, we have explored fluid and solid mechanics in which viscosity does not dissipate energy and elasticity does not store it. Realistic models of complex media will almost always involve additional effects, e.g., antisymmetric stress, other active stresses, coupled fields, and strong

nonlinearities. From the point of view of phenomenological modeling, the virtues of the odd viscosity and odd elasticity formulations lie in their simplicity: They only require deformations as a degree of freedom, and momentum conservation. By combining advances in statistical mechanics, hydrodynamics, dynamical systems, and experimental methods, odd viscosity and odd elasticity may provide a window into the universal behavior of matter at long length scales.

DISCLOSURE STATEMENT

The authors are not aware of any affiliations, memberships, funding, or financial holdings that might be perceived as affecting the objectivity of this review.

ACKNOWLEDGMENTS

We thank Ming Han, Tali Khain, David Martin, and Daniel S. Seara for useful comments and discussions. M.F. acknowledges support from an MRSEC-funded Kadanoff–Rice fellowship (DMR-2011854) and the Simons Foundation. C.S. acknowledges support from the Bloomenthal Fellowship and the National Science Foundation Graduate Research Fellowship under Grant No. 1746045. V.V. acknowledges support from the Simons Foundation, the Complex Dynamics and Systems Program of the Army Research Office under grant W911NF-19-1-0268, the National Science Foundation under grant DMR-2118415, and the University of Chicago Materials Research Science and Engineering Center, which is funded by the National Science Foundation under Award No. DMR-2011854.

LITERATURE CITED

- Truesdell C, Toupin R. 1960. In Principles of Classical Mechanics and Field Theory, ed. S Flügge, pp. 226–858.
 Berlin: Springer-Verlag
- Landau LD, Lifshitz EM. 1959. Fluid Mechanics, Vol. 6, Course of Theoretical Physics. Oxford, UK: Pergamon. 1st ed.
- 3. Landau LD, Lifshitz EM. 1986. Theory of Elasticity, Vol. 7, Course of Theoretical Physics. Oxford, UK: Elsevier. 3rd ed. Transl. JB Sykes, WH Reid (From Russian)
- 4. Khain T, Scheibner C, Fruchart M, Vitelli V. 2022. 7. Fluid Mech. 934:A23
- 5. Avron JE. 1998. *J. Stat. Phys.* 92:543–57
- 6. Han M, Fruchart M, Scheibner C, Vaikuntanathan S, de Pablo JJ, Vitelli V. 2021. Nat. Phys. 17:1260-69
- 7. Condiff DW, Dahler JS. 1964. Phys. Fluids 7:842–54
- 8. Goldhirsch I. 2010. Granular Matter 12:239-52
- 9. Eringen A. 2012. Microcontinuum Field Theories: I. Foundations and Solids. New York: Springer
- 10. de Groot SR, Mazur P. 1954. Phys. Rev. 94:218-24
- 11. de Groot SR, Mazur P. 1962. Non-Equilibrium Thermodynamics. Amsterdam: Dover
- 12. Rao P, Bradlyn B. 2021. arXiv:2112.04545
- 13. Cook CQ, Lucas A. 2021. Phys. Rev. Lett. 127:176603
- 14. Rao P, Bradlyn B. 2020. Phys. Rev. X 10:021005
- 15. Fruchart M, Han M, Scheibner C, Vitelli V. 2022. arXiv:2202.02037
- 16. Schofield P, Henderson JR. 1982. Proc. R. Soc. A. Math. Phys. Sci. 379:231-46
- Irving JH, Kirkwood JG. 1950. J. Chem. Phys. 18:817–29
- 18. Souslov A, Gromov A, Vitelli V. 2020. Phys. Rev. E 101:052606
- 19. Hess S. 1986. 7. Non Equilibrium Thermodyn. 11(3-4):175-94
- 20. Jarkova E, Pleiner H, Müller HW, Fink A, Brand H. 2001. Eur. Phys. J. E 5:583-88
- 21. Varnavides G, Jermyn AS, Anikeeva P, Felser C, Narang P. 2020. Nat. Commun. 11:4710
- 22. Friedman AJ, Cook CQ, Lucas A. 2022. arXiv:2202.08269
- 23. Huang X, Lucas A. 2022. J. High Energy Phys. 2022:82
- 24. Zhao Z, Wang B, Komura S, Yang M, Ye F, Seto R. 2021. Phys. Rev. Res. 3:043229

- 25. Nicolis A, Son DT. 2011. arXiv:1103.2137
- 26. Jensen K, Kaminski M, Kovtun P, Meyer R, Ritz A, Yarom A. 2012. J. High Energy Phys. 2012:102
- 27. Gromov A, Son DT. 2017. Phys. Rev. X 7:041032
- 28. Salbreux G, Jülicher F, Prost J, Callan-Jones A. 2022. Phys. Rev. Res. 4:033158
- 29. Robredo I, Rao P, de Juan F, Bergara A, Mañes JL, et al. 2021. Phys. Rev. Res. 3:1032068
- 30. Banerjee D, Souslov A, Abanov AG, Vitelli V. 2017. Nat. Commun. 8:1573
- 31. Ganeshan S, Abanov AG. 2017. Phys. Rev. Fluids 2:094101
- 32. Guyon E, Hulin J, Petit L, Mitescu C. 2015. Physical Hydrodynamics. Oxford, UK: Oxford Univ. Press
- 33. Beenakker JJM, McCourt FR. 1970. Annu. Rev. Phys. Chem. 21:47-72
- McCourt F. 1990. Nonequilibrium Phenomena in Polyatomic Gases. New York/Oxford: Clarendon/Oxford Univ. Press
- 35. Korving J, Hulsman H, Knaap H, Beenakker J. 1966. Phys. Lett. 21:5-7
- 36. Korving J, Hulsman H, Scoles G, Knaap H, Beenakker J. 1967. Physica 36:177-97
- 37. Hulsman H, Knaap H. 1970. Physica 50:565-72
- 38. Hulsman H, Van Waasdijk E, Burgmans A, Knaap H, Beenakker J. 1970. Physica 50:53-76
- 39. Banerjee D, Souslov A, Vitelli V. 2022. Phys. Rev. Fluids 7:043301
- 40. Souslov A, Dasbiswas K, Fruchart M, Vaikuntanathan S, Vitelli V. 2019. Phys. Rev. Lett. 122:128001
- 41. Reynolds D, Monteiro GM, Ganeshan S. 2021. arXiv:2112.03076
- 42. Holder T, Queiroz R, Stern A. 2019. Phys. Rev. Lett. 123:106801
- 43. Delacrétaz LV, Gromov A. 2017. Phys. Rev. Lett. 119:226602
- 44. Hosaka Y, Komura S, Andelman D. 2021. Phys. Rev. E 104:064613
- Tropea C, Yarin AL, Foss JF. 2007. Springer Handbook of Experimental Fluid Mechanics. Berlin/Heidelberg: Springer
- 46. Ariman T, Turk M, Sylvester N. 1973. Int. 7. Eng. Sci. 11:905-30
- Hess S. 2019. Atti Della Accademia Peloritana dei Pericolanti: Classe di Scienze Fisiche, Matematiche e Naturali 97(Suppl. 1):A9
- 48. Kiselev EI, Schmalian J. 2019. Phys. Rev. B 99:035430
- 49. Lucas A, Fong KC. 2018. 7. Phys. Condens. Matter 30:053001
- 50. Tsai JC, Ye F, Rodriguez J, Gollub JP, Lubensky T. 2005. Phys. Rev. Lett. 94:214301
- 51. van Zuiden BC, Paulose J, Irvine WTM, Bartolo D, Vitelli V. 2016. PNAS 113:12919-24
- 52. Soni V, Bililign ES, Magkiriadou S, Sacanna S, Bartolo D, et al. 2019. Nat. Phys. 15:1188-94
- 53. Abanov A, Can T, Ganeshan S. 2018. SciPost Phys. 5:010
- 54. Abanov AG, Can T, Ganeshan S, Monteiro GM. 2020. Phys. Rev. Fluids 5:104802
- 55. Bogatskiy A, Wiegmann P. 2019. Phys. Rev. Lett. 122:214505
- 56. Tauber C, Delplace P, Venaille A. 2019. J. Fluid Mech. 868:R2
- 57. Baardink G, Cassella G, Neville L, Milewski PA, Souslov A. 2021. Phys. Rev. E 104:014603
- 58. Shankar S, Souslov A, Bowick MJ, Marchetti MC, Vitelli V. 2022. Nat. Rev. Phys. 4:380–98
- 59. Fruchart M, Carpentier D. 2013. C. R. Phys. 14:779-815
- 60. Kogan E. 2016. Phys. Rev. E 94:043111
- 61. Lapa MF, Hughes TL. 2014. Phys. Rev. E 89:043019
- 62. Lier R, Duclut C, Bo S, Armas J, Jülicher F, Surówka P. 2022. arXiv:2205.12704
- Kim S, Karrila SJ. 1991. Microbydrodynamics: Principles and Selected Applications. Oxford, UK: Butterworth-Heinemann
- Happel J, Brenner H. 2012. Low Reynolds Number Hydrodynamics: With Special Applications to Particulate Media. Dordrecht, Neth.: Springer
- 65. Masoud H, Stone HA. 2019. 7. Fluid Mech. 879:P1
- 66. Hosaka Y, Komura S, Andelman D. 2021. Phys. Rev. E 103:042610
- Charru F. 2011. Hydrodynamic Instabilities. Cambridge, UK: Cambridge Univ. Press. Transl. P de Forcrand–Millard
- 68. Faganello M, Califano F. 2017. J. Plasma Phys. 83(6):535830601
- 69. Nagano H. 1979. Planet. Space Sci. 27:881-84
- 70. Wolff RS, Goldstein BE, Yeates CM. 1980. 7. Geophys. Res. 85:7697-707

- 71. Lucas A, Surówka P. 2014. Phys. Rev. E 90:063005
- 72. Kirkinis E, Andreev AV. 2019. 7. Fluid Mech. 878:169-89
- 73. Bao G, Jian Y. 2021. Phys. Rev. E 103:013104
- 74. Chattopadhyay S. 2021. Phys. Fluids 33:062106
- 75. Samanta A. 2022. J. Fluid Mech. 938:A9
- Rosenbluth MN, Krall NA, Rostoker N. 1962. Nuclear Fusion: 1962 Suppl., Pt. 1, Conf. Pap. No. CN-10/170, Int. Atomic Energy Agency, Vienna, Aust.
- Newcomb WA, U.S. At. Energy Comm., Lawrence Radiat. Lab. 1966. Dynamics of a gyroviscous plasma. Livermore, California: Univ. Calif., Lawrence Radiat. Lab.
- 78. Roberts KV, Taylor JB. 1962. Phys. Rev. Lett. 8:197–98
- Pottier N. 2010. Nonequilibrium Statistical Physics: Linear Irreversible Processes. Oxford, UK: Oxford Univ. Press
- 80. Callen HB. 1985. Thermodynamics and an Introduction to Thermostatistics. New York: John Wiley & Sons
- 81. Epstein JM, Mandadapu KK. 2020. Phys. Rev. E 101:052614
- 82. Hargus C, Klymko K, Epstein JM, Mandadapu KK. 2020. J. Chem. Phys. 152:201102
- 83. Bradlyn B, Goldstein M, Read N. 2012. Phys. Rev. B 86:245309
- 84. Read N, Rezayi EH. 2011. Phys. Rev. B 84:085316
- 85. Offertaler B, Bradlyn B. 2019. Phys. Rev. B 99:035427
- 86. Krommes JA, Hu G. 1993. Phys. Fluids B: Plasma Phys. 5:3908-41
- 87. Coleman BD, Truesdell C. 1960. J. Chem. Phys. 33:28-31
- 88. Berdyugin AI, Xu SG, Pellegrino FMD, Kumar RK, Principi A, et al. 2019. Science 364(6436):162-65
- 89. ten Bosch B, Beenakker J, Kuščer I. 1984. Phys. A Stat. Mech. Appl. 123:443-62
- 90. Sharipov F. 1994. Phys. A Stat. Mech. Appl. 203:437-56
- 91. Sharipov F. 1994. Phys. A Stat. Mech. Appl. 203:457–85
- 92. Yamauchi L, Hayata T, Uwamichi M, Ozawa T, Kawaguchi K. 2020. arXiv:2008.10852
- Barabanov AF, Kagan YM, Maksimov LA, Mikheyenkov AV, Khabarova TV. 2015. Physics-Uspekhi 58:446–54
- 94. Strohm C, Rikken GLJA, Wyder P. 2005. Phys. Rev. Lett. 95:155901
- 95. Koch DL, Brady JF. 1987. Phys. Fluids 30:642-50
- 96. Auriault JL, Moyne C, Amaral Souto HP. 2010. Transport Porous Media 85:771-83
- 97. Hargus C, Epstein JM, Mandadapu KK. 2021. Phys. Rev. Lett. 127:178001
- 98. Vega Reyes F, López-Castaño MA, Rodríguez-Rivas A. 2022. Commun. Phys. 5:256
- 99. Rikken GLJA, van Tiggelen BA. 1996. Nature 381:54-55
- 100. van Tiggelen BA. 1995. Phys. Rev. Lett. 75:422-24
- 101. Quan L, Yves S, Peng Y, Esfahlani H, Alù A. 2021. Nat. Commun. 12:2615
- Chaikin PM, Lubensky TC. 1995. Principles of Condensed Matter Physics. Cambridge, UK: Cambridge Univ. Press
- 103. Anderson PW, ed. 1984. Basic Notions of Condensed Matter Physics. Boca Raton, FL: CRC
- 104. Kole SJ, Alexander GP, Ramaswamy S, Maitra A. 2021. Phys. Rev. Lett. 126:248001
- 105. Maitra A, Lenz M, Voituriez R. 2020. Phys. Rev. Lett. 125:238005
- 106. Korving J, Hulsman H, Hermans L, de Groot J, Knaap H, Beenakker J. 1966. 7. Mol. Spectrosc. 20:294–95
- Chapman S, Cowling T. 1990. The Mathematical Theory of Non-Uniform Gases: An Account of the Kinetic Theory of Viscosity, Thermal Conduction and Diffusion in Gases. Cambridge, UK: Cambridge Univ. Press. 3rd ed.
- 108. Braginskii SI. 1958. Sov. Phys. 7. Exp. Theor. Phys. 6:358-69
- 109. Braginskii SI. 1965. Rev. Plasma Phys. 1:205-311
- 110. Ramos JJ. 2005. Phys. Plasmas 12:112301
- 111. Kaufman AN. 1960. Phys. Fluids 3:610–16
- 112. Steinhauer LC. 2011. Phys. Plasmas 18:070501
- 113. Stasiewicz K. 1993. Space Sci. Rev. 65:221-52
- 114. Nayyar NK, Trehan SK. 1970. 7. Plasma Phys. 4:563-71
- 115. Steinhauer LC, Ishida A. 1990. Phys. Fluids B: Plasma Phys. 2:2422-30

- 116. Terada N, Machida S, Shinagawa H. 2002. 7. Geophys. Res. Space Phys. 107:SMP 30
- 117. Ishizawa A, Horiuchi R. 2005. Phys. Rev. Lett. 95:045003
- 118. Ferraro NM, Jardin SC. 2006. Phys. Plasmas 13:092101
- 119. Bae C, Stacey W, Solomon W. 2013. Nuclear Fusion 53:043011
- 120. Stacey WM, Sigmar DJ. 1985. Phys. Fluids 28:2800-7
- 121. Stacey WM, Mandrekas J. 2002. Phys. Plasmas 9:1622-28
- 122. Stacey WM, Johnson RW, Mandrekas J. 2006. Phys. Plasmas 13:062508
- 123. Winske D. 1996. Phys. Plasmas 3:3966-74
- 124. Zhu P, Schnack DD, Ebrahimi F, Zweibel EG, Suzuki M, et al. 2008. Phys. Rev. Lett. 101:085005
- 125. Yajima N. 1966. Prog. Theor. Phys. 36:1-16
- 126. Nakagawa Y. 1956. 7. Phys. Earth 4:105-11
- 127. Sulpizio JA, Ella L, Rozen A, Birkbeck J, Perello DJ, et al. 2019. Nature 576:75-79
- 128. Ku MJH, Zhou TX, Li Q, Shin YJ, Shi JK, et al. 2020. Nature 583:537-41
- 129. Bandurin DA, Torre I, Kumar RK, Ben Shalom M, Tomadin A, et al. 2016. Science 351:1055-58
- 130. Moll PJW, Kushwaha P, Nandi N, Schmidt B, Mackenzie AP. 2016. Science 351:1061-64
- 131. Crossno J, Shi JK, Wang K, Liu X, Harzheim A, et al. 2016. Science 351:1058–61
- 132. de Jong MJM, Molenkamp LW. 1995. Phys. Rev. B 51:13389-402
- 133. Zaanen J. 2016. Science 351:1026-27
- 134. Vollhardt D, Wolfle P. 2013. The Superfluid Phases of Helium 3. New York: Dover
- 135. Volovik GE. 2020. J. Low Temp. Phys. 202:11-28
- 136. Furusawa T, Fujii K, Nishida Y. 2021. Phys. Rev. B 103:064506
- 137. Fujii K, Nishida Y. 2018. Ann. Phys. 395:170-82
- 138. Read N. 2009. Phys. Rev. B 79:045308
- 139. Avron JE, Seiler R, Zograf PG. 1995. Phys. Rev. Lett. 75:697–700
- 140. Haldane FDM. 2009. arXiv:0906.1854
- 141. Haldane FDM. 2011. Phys. Rev. Lett. 107:116801
- 142. Park Y, Haldane FDM. 2014. Phys. Rev. B 90:045123
- 143. Hoyos C, Son DT. 2012. Phys. Rev. Lett. 108:066805
- 144. Fürthauer S, Strempel M, Grill SW, Jülicher F. 2012. Eur. Phys. J. E 35:89
- 145. Markovich T, Tjhung E, Cates ME. 2019. New J. Phys. 21:112001
- 146. Yeo K, Lushi E, Vlahovska PM. 2015. Phys. Rev. Lett. 114:188301
- 147. Grzybowski BA, Stone HA, Whitesides GM. 2000. Nature 405:1033-36
- 148. Yan J, Bae SC, Granick S. 2015. Soft Matter 11:147-53
- 149. Bililign ES, Balboa Usabiaga F, Ganan YA, Poncet A, Soni V, et al. 2021. Nat. Phys. 18(2):212-18
- 150. Denk J, Huber L, Reithmann E, Frey E. 2016. Phys. Rev. Lett. 116:178301
- 151. Liebchen B, Levis D. 2017. Phys. Rev. Lett. 119:058002
- López-Castaño MA, Seco AM, Seco AM, Álvaro Rodríguez-Rivas, Reyes FV. 2022. Phys. Rev. Res. 4:033230
- 153. Scholz C, Engel M, Pöschel T. 2018. Nat. Commun. 9:931
- 154. Yang X, Ren C, Cheng K, Zhang HP. 2020. Phys. Rev. E 101:022603
- 155. Riedel IH, Kruse K, Howard J. 2005. Science 309:300-3
- 156. Petroff AP, Wu XL, Libchaber A. 2015. Phys. Rev. Lett. 114:158102
- 157. Tan TH, Mietke A, Li J, Chen Y, Higinbotham H, et al. 2022. Nature 607:287-93
- 158. Markovich T, Lubensky TC. 2021. Phys. Rev. Lett. 127:048001
- 159. Zhao Z, Yang M, Komura S, Seto R. 2022. Front. Phys. 10:951465
- 160. Garzó V. 2017. Phys. Rev. E 95:062906
- 161. Wiegmann P, Abanov AG. 2014. Phys. Rev. Lett. 113:034501
- 162. Yu X, Bradley AS. 2017. Phys. Rev. Lett. 119:185301
- 163. Moroz S, Hoyos C, Benzoni C, Son DT. 2018. SciPost Phys. 5:039
- 164. Reichhardt CJO, Reichhardt C. 2022. EuroPhys. Lett. 137:66004
- 165. Goldston RJ. 2020. Introduction to Plasma Physics. Boca Raton, FL: CRC
- 166. Hazeltine R. 2018. The Framework of Plasma Physics. Boca Raton, FL: CRC

- 167. Kagan Y, Maksimov L. 1962. 7. Exp. Theor. Phys. Lett. 14:604-10
- 168. Kagan Y, Afanasév AM. 1962. J. Exp. Theor. Phys. Lett. 14:1096-101
- Kagan Y, Maksimov L. 1967. J. Exp. Theor. Phys. Lett. 24:1893–908
- 170. Moraal H, McCourt F, Knaap HFP. 1969. Physica 45:455-68
- 171. McCourt F, Knaap H, Moraal H. 1969. Physica 43:485-512
- 172. Knaap H, Beenakker J. 1967. Physica 33:643-70
- 173. McCourt FR, Snider RF. 1967. 7. Chem. Phys. 47:4117-28
- 174. Levi A, McCourt F. 1968. Physica 38:415-37
- 175. Waldmann L. 1958. Z. Naturforsch. A 13:609-20
- 176. Hess S. 2003. Z. Naturforsch. A 58:269-74
- 177. Harris S. 2004. An Introduction to the Theory of the Boltzmann Equation. New York: Dover
- Dorfman J, van Beijeren H, Kirkpatrick T. 2021. Contemporary Kinetic Theory of Matter. Cambridge, UK: Cambridge Univ. Press
- 179. Morrison PJ. 1998. Rev. Mod. Phys. 70:467-521
- 180. Salmon R. 1988. Ann. Rev. Fluid Mech. 20:225-56
- 181. Morrison PJ, Caldas IL, Tasso H. 1984. Z. Naturforsch. A 39:1023-27
- 182. Lingam M, Morrison P. 2014. Phys. Lett. A 378:3526-32
- 183. Morrison PJ. 2005. Phys. Plasmas 12:058102
- 184. Morrison PJ, Lingam M, Acevedo R. 2014. Phys. Plasmas 21:082102
- 185. Lingam M, Morrison PJ, Wurm A. 2020. *J. Plasma Phys.* 86:835860501
- 186. Lingam M. 2015. Phys. Lett. A 379:1425-30
- 187. Monteiro GM, Abanov AG, Ganeshan S. 2021. arXiv:2105.01655
- 188. Wen XG, Zee A. 1992. Phys. Rev. Lett. 69:953-56
- 189. Abanov AG, Gromov A. 2014. Phys. Rev. B 90:014435
- 190. Hughes TL, Leigh RG, Parrikar O. 2013. Phys. Rev. D 88:025040
- 191. Gromov A, Jensen K, Abanov AG. 2016. Phys. Rev. Lett. 116:126802
- 192. Geracie M, Son DT. 2014. J. High Energy Phys. 2014:4
- 193. Haehl FM, Loganayagam R, Rangamani M. 2015. J. High Energy Phys. 2015:60
- 194. Scheibner C, Souslov A, Banerjee D, Surówka P, Irvine WTM, Vitelli V. 2020. Nat. Phys. 16:475–80
- 195. Scheibner C, Irvine WTM, Vitelli V. 2020. Phys. Rev. Lett. 125:118001
- 196. Shankar S, Mahadevan L. 2022. bioRxiv 2022.02.20.481216
- 197. Braverman L, Scheibner C, VanSaders B, Vitelli V. 2021. Phys. Rev. Lett. 127:268001
- 198. Nelson D, Halperin B. 1979. Phys. Rev. B 19:2457-84
- 199. Ashida Y, Gong Z, Ueda M. 2020. Adv. Phys. 69:249-435
- Zubov LM. 1997. Nonlinear Theory of Dislocations and Disclinations in Elastic Bodies, Vol. 47, Lect. Notes Phys. Monogr. Berlin/Heidelberg: Springer
- 201. Marsden JE. 1994. Mathematical Foundations of Elasticity. New York: Dover
- 202. Truesdell CA. 1963. J. Res. Natl. Bureau Standards Sect. B Math. Math. Phys. 67B(2):85
- 203. Nassar H, Yousefzadeh B, Fleury R, Ruzzene M, Alù A, et al. 2020. Nat. Rev. Mater. 5:667-85
- Rice JR. 1976. In Theoretical and Applied Mechanics (Proceedings of the 14th International Congress on Theoretical and Applied Mechanics, Vol. 1), ed. WT Koiter, pp. 207–20. Delft, Neth.: North Holland
- 205. La Ragione L, Oger L, Recchia G, Sollazzo A. 2015. Proc. R. Soc. A Math. Phys. Eng. Sci. 471:20150013
- 206. Örs H, Prévost JH. 1995. Acta Mech. 111:181-92
- 207. Prévost JH. 1982. Int. J. Numer. Anal. Methods Geomechan. 6:323-38
- 208. Piccolroaz A, Bigoni D, Willis JR. 2006. J. Mech. Phys. Solids 54:2391-417
- 209. Bigoni D. 1995. Int. J. Solids Struct. 32:3167-89
- 210. Bordiga G, Piccolroaz A, Bigoni D. 2022. J. Mech. Phys. Solids 158:104665
- 211. Carol I, Willam K. 1996. Int. 7. Solids Struct. 33:2939-57
- 212. Carol I, Jirásek M, Bažant Z. 2001. Int. 7. Solids Struct. 38:2921-31
- 213. Challamel N, Halm D, Dragon A. 2006. C. R. Mécan. 334:414-18
- 214. Lubensky TC. 2005. Pramana J. Phys. 64:727–42
- Warner M, Terentjev EM. 2003. Liquid Crystal Elastomers, Vol. 120, Int. Ser. Monogr. Phys. Oxford, UK: Oxford Univ. Press

- 216. Storm C, Pastore JJ, MacKintosh FC, Lubensky TC, Janmey PA. 2005. Nature 435:191-94
- 217. Cosserat E, Cosserat F. 1909. Théorie des Corps Déformables. Paris: A. Hermann et Fils
- 218. Lakes RS, Benedict RL. 1982. Int. J. Eng. Sci. 20:1161-67
- 219. Chen Y, Li X, Scheibner C, Vitelli V, Huang G. 2021. Nat. Commun. 12:5935
- 220. Brandenbourger M, Scheibner C, Veenstra J, Vitelli V, Coulais C. 2021. arXiv:2108.08837
- Palacci J, Sacanna S, Kim SH, Yi GR, Pine DJ, Chaikin PM. 2014. Philos. Trans. R. Soc. A Math. Phys. Eng. Sci. 372:20130372
- 222. Briand G, Schindler M, Dauchot O. 2018. Phys. Rev. Lett. 120:208001
- 223. Desreumaux N, Florent N, Lauga E, Bartolo D. 2012. Eur. Phys. J. E 35:68
- 224. Lavergne FA, Wendehenne H, Bäuerle T, Bechinger C. 2019. Science 364:70–74
- 225. Baconnier P, Shohat D, Hernández López C, Coulais C, Démery V, et al. 2022. Nat. Phys. 18:1234–39
- 226. Guazzelli É, Hinch J. 2011. Annu. Rev. Fluid Mech. 43:97-116
- 227. Beatus T, Bar-Ziv R, Tlusty T. 2007. Phys. Rev. Lett. 99:124502
- 228. Beatus T, Tlusty T, Bar-Ziv R. 2006. Nat. Phys. 2:743-48
- 229. Baek Y, Solon AP, Xu X, Nikola N, Kafri Y. 2018. Phys. Rev. Lett. 120:058002
- 230. Uchida N, Golestanian R. 2010. Phys. Rev. Lett. 104:178103
- 231. Soto R, Golestanian R. 2014. Phys. Rev. Lett. 112:068301
- 232. Saha S, Ramaswamy S, Golestanian R. 2019. New J. Phys. 21:063006
- 233. Meredith CH, Moerman PG, Groenewold J, Chiu YJ, Kegel WK, et al. 2020. Nat. Chem. 12:1136-42
- 234. Ivlev AV, Bartnick J, Heinen M, Du CR, Nosenko V, Löwen H. 2015. Phys. Rev. X 5:011035
- 235. Peterson CW, Parker J, Rice SA, Scherer NF. 2019. Nano Lett. 19:897-903
- 236. Yifat Y, Coursault D, Peterson CW, Parker J, Bao Y, et al. 2018. Light Sci. Appl. 7:105
- 237. Han F, Parker JA, Yifat Y, Peterson C, Gray SK, et al. 2018. Nat. Commun. 9:4897
- 238. Poncet A, Bartolo D. 2022. Phys. Rev. Lett. 128:048002
- 239. Nash LM, Kleckner D, Read A, Vitelli V, Turner AM, Irvine WTM. 2015. PNAS 112:14495-500
- Bauer A, Pfleiderer C. 2016. In Topological Structures in Ferroic Materials, Vol. 228, Springer Ser. Mater. Sci., ed. J Seidel, pp. 1–28. Cham: Springer Int.
- 241. Koschmieder E, Pallas S. 1974. Int. J. Heat Mass Transf. 17:991-1002
- 242. Born M, Huang K. 1954. Dynamical Theory of Crystal Lattices. Oxford, UK: Clarendon
- 243. Lutsko JF. 1989. J. Appl. Phys. 65:2991–97
- Barrat J-L. 2006. In Computer Simulations in Condensed Matter Systems: From Materials to Chemical Biology, Vol. 2, Lect. Notes Phys., Vol. 704, ed. M Ferraria, G Coccotti, K Binder, pp. 287–307. Berlin/Heidelberg: Springer
- 245. Fruchart M, Vitelli V. 2020. Phys. Rev. Lett. 124:248001
- 246. Chen Z. 2022. arXiv:2204.06587
- 247. Wang P, Lu L, Bertoldi K. 2015. Phys. Rev. Lett. 115:104302
- 248. Zhao Y, Zhou X, Huang G. 2020. J. Mech. Phys. Solids 143:104065
- 249. Carta G, Brun M, Movchan A, Movchan N, Jones I. 2014. Int. J. Solids Struct. 51:2213-25
- 250. Hassanpour S. 2014. Dynamics of gyroelastic continua. PhD Thesis, Univ. Waterloo
- 251. Carta G, Jones IS, Movchan NV, Movchan AB, Nieves MJ. 2017. Sci. Rep. 7:26
- 252. Mitchell NP, Nash LM, Irvine WTM. 2018. Phys. Rev. B 98:174301
- 253. Mitchell NP, Nash LM, Irvine WTM. 2018. Phys. Rev. B 97:100302
- 254. Mitchell NP, Nash LM, Hexner D, Turner AM, Irvine WTM. 2018. Nat. Phys. 14:380-85
- 255. Brun M, Jones IS, Movchan AB. 2012. Proc. R. Soc. A Math. Phys. Eng. Sci. 468:3027-46
- 256. Benzoni C, Jeevanesan B, Moroz S. 2021. Phys. Rev. B 104:024435
- 257. Huang P, Schönenberger T, Cantoni M, Heinen L, Magrez A, et al. 2020. Nat. Nanotechnol. 15:761-67
- 258. Ochoa H, Kim SK, Tchernyshyov O, Tserkovnyak Y. 2017. Phys. Rev. B 96:020410
- 259. Mühlbauer S, Binz B, Jonietz F, Pfleiderer C, Rosch A, et al. 2009. Science 323:915-19
- 260. Yu XZ, Onose Y, Kanazawa N, Park JH, Han JH, et al. 2010. Nature 465:901-4
- 261. Brearton R, Turnbull LA, Verezhak JAT, Balakrishnan G, Hatton PD, et al. 2021. Nat. Commun. 12:2723
- 262. Sonin EB. 1987. Rev. Mod. Phys. 59:87-155
- 263. Gifford SA, Baym G. 2008. Phys. Rev. A 78:043607

- 264. Nguyen DX, Gromov A, Moroz S. 2020. SciPost Phys. 9:76
- 265. Moroz S, Hoyos C, Benzoni C, Son DT. 2018. SciPost Phys. 5:39
- 266. Fetter AL. 2009. Rev. Mod. Phys. 81:647-91
- 267. Blatter G, Feigel'man MV, Geshkenbein VB, Larkin AI, Vinokur VM. 1994. Rev. Mod. Phys. 66:1125-388
- 268. Tkachenko VK. 1969. 7. Exp. Theor. Phys. 29:945
- 269. Tkachenko V. 1966. Sov. Phys. J. Exp. Theor. Phys. 22:1282-86
- 270. Tkachenko V. 1966. Sov. Phys. J. Exp. Theor. Phys. 23:1049-56
- 271. Petroff AP, Wu XL, Libchaber A. 2015. Phys. Rev. Lett. 114:158102
- 272. Drescher K, Leptos KC, Tuval I, Ishikawa T, Pedley TJ, Goldstein RE. 2009. Phys. Rev. Lett. 102:168101
- 273. Goldman A, Cox R, Brenner H. 1967. Chem. Eng. Sci. 22:637-51
- 274. Happel J, Brenner H. 1981. Low Reynolds Number Hydrodynamics: With Special Applications to Particulate Media, Mechanics of Fluids and Transport Processes. Dordrecht, Neth.: Springer
- 275. Jäger S, Klapp SHL. 2011. Soft Matter 7:6606-16
- 276. Timoshenko S. 1940. Strength of Materials. New York: D. Van Nostrand Co. 2nd ed.
- 277. Cheng W, Hu G. 2021. Sci. China Phys., Mech. Astron. 64(11):114612
- 278. Salbreux G, Jülicher F. 2017. Phys. Rev. E 96:032404
- 279. Fossati M, Scheibner C, Fruchart M, Vitelli V. 2022. arXiv:2210.03669 [cond-mat.soft]
- 280. Zahalak GI. 1996. J. Theor. Biol. 182:59-84
- 281. Cross MC, Meiron D, Tu Y. 1994. Chaos Interdiscip. 7. Nonlinear Sci. 4:607-19
- Cross M, Greenside H. 2009. Pattern Formation and Dynamics in Nonequilibrium Systems. Cambridge, UK: Cambridge Univ. Press
- 283. Pismen L. 2010. Patterns and Interfaces in Dissipative Dynamics. Berlin/Heidelberg: Springer
- 284. Busse FH, Heikes KE. 1980. Science 208:173-75
- 285. Bodenschatz E, Pesch W, Ahlers G. 2000. Annu. Rev. Fluid Mech. 32:709-78
- 286. Ahlers G. 2006. Springer Tracts Mod. Phys. 207:67-94
- 287. Guarino A, Vidal V. 2004. Phys. Rev. E 69:066311
- 288. Fruchart M, Hanai R, Littlewood PB, Vitelli V. 2021. Nature 592:363-69
- 289. Nardini C, Fodor E, Tjhung E, van Wijland F, Tailleur J, Cates ME. 2017. Phys. Rev. X 7:021007
- Wittkowski R, Tiribocchi A, Stenhammar J, Allen RJ, Marenduzzo D, Cates ME. 2014. Nat. Commun. 5:4351
- 291. Kozyreff G, Tlidi M. 2007. Chaos: Interdiscip. 7. Nonlinear Sci. 17:037103
- 292. Coullet P, Lega J, Houchmanzadeh B, Lajzerowicz J. 1990. Phys. Rev. Lett. 65:1352-55
- 293. Coullet P, Goldstein RE, Gunaratne GH. 1989. Phys. Rev. Lett. 63:1954-57
- 294. Pomeau Y, Zaleski S, Manneville P. 1983. Phys. Rev. A 27:2710-26
- Bodenschatz E, Cannell DS, de Bruyn JR, Ecke R, Hu YC, et al. 1992. Phys. D: Nonlinear Phenom. 61:77– 93
- 296. Clerc MG, Petrossian A, Residori S. 2005. Phys. Rev. E 71:015205
- 297. Siggia ED, Zippelius A. 1981. Phys. Rev. A 24:1036-49
- 298. Colinet P, Nepomnyashchy AA, Legros JC. 2002. Europhys. Lett. 57:480–86
- 299. Tsimring LS. 1996. Phys. D Nonlinear Phenom. 89:368-80
- 300. Houghton SM, Knobloch E. 2011. Phys. Rev. E 84:016204
- 301. You Z, Baskaran A, Marchetti MC. 2020. PNAS 117:19767-72
- 302. Saha S, Agudo-Canalejo J, Golestanian R. 2020. Phys. Rev. X 10:041009
- 303. Frohoff-Hülsmann T, Holl MP, Knobloch E, Gurevich SV, Thiele U. 2022. arXiv:2205.14364
- 304. Clerc MG, Verschueren N. 2013. Phys. Rev. E 88:052916
- 305. Coullet P, Emilsson K. 1992. Phys. D Nonlinear Phenom. 61:119-31
- 306. Cates ME. 2019. arXiv:1904.01330
- 307. Loos SAM, Hermann SM, Klapp SHL. 2019. arXiv:1910.08372
- 308. Loos SAM, Klapp SHL. 2020. New 7. Phys. 22:123051
- 309. Echebarria B, Pérez-García C. 1998. Europhys. Lett. 43:35-40
- 310. Echebarria B, Riecke H. 2000. Phys. D Nonlinear Phenom. 139:97-108
- 311. Echebarria B, Riecke H. 2000. Phys. D Nonlinear Phenom. 143:187-204

- 312. Marder M. 2010. Condensed Matter Physics. Hoboken, NJ: John Wiley & Sons
- Nelson DR. 2002. Defects and Geometry in Condensed Matter Physics. Cambridge/New York: Cambridge Univ. Press
- 314. Weertman J, Weertman JR. 1964. Elementary Dislocation Theory. New York: Macmillan
- 315. Ishimoto K, Moreau C, Yasuda K. 2022. Phys. Rev. E 105:064603
- 316. Zhou D, Zhang J. 2020. Phys. Rev. Res. 2:023173
- 317. Strogatz S. 2019. Nonlinear Dynamics and Chaos: With Applications to Physics, Biology, Chemistry, and Engineering. Boca Raton, FL: CRC
- Tedrake R. 2022. Underactuated robotics: algorithms for walking, running, swimming, flying, and manipulation. Course Notes for MIT 6.832, Mass. Inst. Technol., Cambridge. Accessed Oct. 10. https://underactuated.csail.mit.edu/
- 319. Yasuda K, Hosaka Y, Sou I, Komura S. 2021. J. Phys. Soc. Jpn. 90:075001
- 320. Yasuda K, Kobayashi A, Lin LS, Hosaka Y, Sou I, Komura S. 2022. J. Phys. Soc. Jpn. 91:015001
- 321. Yasuda K, Ishimoto K, Kobayashi A, Lin LS, Sou I, et al. 2022. J. Chem. Phys. 157:095101
- 322. Oswald P. 2014. Rheophysics: The Deformation and Flow of Matter. Cambridge, UK: Cambridge Univ. Press
- Landau LD, Lifshitz EM. 1984. Electrodynamics of Continuous Media, Vol. 8, Course of Theoretical Physics. Oxford, UK: Pergamon. 2nd ed. Transl. JB Sykes, JS Bell, MJ Kearsley (From Russian)
- 324. Banerjee D, Vitelli V, Jülicher F, Surówka P. 2021. Phys. Rev. Lett. 126:138001
- 325. Muhlestein MB, Sieck CF, Alù A, Haberman MR. 2016. Proc. R. Soc. A Math. Phys. Eng. Sci. 472:20160604
- 326. Day WA. 1971. Arch. Ration. Mech. Anal. 40:155-59
- 327. Srivastava A. 2015. Proc. R. Soc. A Math. Phys. Eng. Sci. 471:20150256
- 328. Lier R, Armas J, Bo S, Duclut C, Jülicher F, Surówka P. 2022. Phys. Rev. E 105:054607



Contents

Annual Review of Condensed Matter Physics

Volume 14, 2023

A Journey Through Nonlinear Dynamics: The Case of Temperature Gradients Albert Libchaber
An Adventure into the World of Soft Matter Dominique Langevin
Floquet States in Open Quantum Systems Takashi Mori
Generalized Symmetries in Condensed Matter *John McGreevy**
Non-Hermitian Topological Phenomena: A Review Nobuyuki Okuma and Masatoshi Sato
Modeling Active Colloids: From Active Brownian Particles to Hydrodynamic and Chemical Fields Andreas Zöttl and Holger Stark 109
Spin Seebeck Effect: Sensitive Probe for Elementary Excitation, Spin Correlation, Transport, Magnetic Order, and Domains in Solids Takashi Kikkawa and Eiji Saitoh
Superconductivity and Local Inversion-Symmetry Breaking Mark H. Fischer, Manfred Sigrist, Daniel F. Agterberg, and Youichi Yanase
Tensor Network Algorithms: A Route Map Mari Carmen Bañuls
Spatial and Temporal Organization of Chromatin at Small and Large Scales Helmut Schiessel
Dissecting Flux Balances to Measure Energetic Costs in Cell Biology: Techniques and Challenges Easun Arunachalam, William Ireland, Xingbo Yang, and Daniel Needleman
Data-Driven Discovery of Robust Materials for Photocatalytic Energy Conversion Arunima K. Singh, Rachel Gorelik, and Tathagata Biswas

A. Alexandradinata and Leonid Glazman	61
Physics of Human Crowds *Alessandro Corbetta and Federico Toschi** 31	11
Random Quantum Circuits Matthew P.A. Fisher, Vedika Khemani, Adam Nahum, and Sagar Vijay	35
Swimming in Complex Fluids Saverio E. Spagnolie and Patrick T. Underhill	81
Learning Without Neurons in Physical Systems Menachem Stern and Arvind Murugan	17
Quantum Many-Body Scars: A Quasiparticle Perspective Anushya Chandran, Thomas Iadecola, Vedika Khemani, and Roderich Moessner	43
Odd Viscosity and Odd Elasticity Michel Fruchart, Colin Scheibner, and Vincenzo Vitelli	71

Errata

An online log of corrections to *Annual Review of Condensed Matter Physics* articles may be found at http://www.annualreviews.org/errata/conmatphys